Quaternary Science Reviews 267 (2021) 107096

Contents lists available at ScienceDirect

Quaternary Science Reviews

journal homepage: www.elsevier.com/locate/quascirev

The effect of coastal landform development on decadal-to millennial-scale longshore sediment fluxes: Evidence from the Holocene evolution of the central mid-Atlantic coast, USA

Justin L. Shawler [a, *], Christopher J. Hein [a], Chloe A. Obara [b], Mahina G. Robbins [b], Sebastien Huot [c], Michael S. Fenster [d]

[a] Virginia Institute of Marine Science, William & Mary, Gloucester Point, VA, USA
[b] Department of Geology, William & Mary, Williamsburg, VA, USA
[c] Illinois State Geological Survey, Prairie Research Institute, University of Illinois at Urbana-Champaign, Champaign, IL, USA
[d] Environmental Studies Program, Randolph-Macon College, Ashland, VA, USA

ARTICLE INFO

Article history:
Received 20 January 2021
Received in revised form
11 July 2021
Accepted 11 July 2021

Handling Editor: I Hendy

Keywords:
Barrier island
Sediment supply
Sediment sink
Progradation
Longshore transport
Virginia barrier islands

ABSTRACT

The behavior of siliciclastic coastal systems is largely controlled by the interplay between accommodation creation and infilling. Factors responsible for altering sediment fluxes to and along open-ocean coasts include cross-shore mobilization of sediment primarily from tidal currents and storms as well as changes in alongshore transport rates moderated by changing wave conditions, river sediment inputs, artificial shoreline hardening and modification, and natural sediment trapping in updrift coastal landforms. This paper focuses on the latter relationships. To address understudied interactions between updrift coastal landforms and downdrift coastal behavior, we quantify the volume and fluxes of sediment trapped in the Assateague-Chincoteague-Wallops barrier-island complex along the Virginia, USA coast and relate these volumes to downdrift coastal-system behavior. During the last *ca.* 2250 years, these barriers trapped 216 million m^3 of sand through the growth of complex beach- and foredune-ridge systems. A period (*ca.* 400 to 190 years ago) of reduced/no progradation on Chincoteague and Assateague islands corresponds with sediment sequestration in updrift flood-tidal deltas. This finding emphasizes the important control of tidal inlets on alongshore sediment fluxes on barrier-island coasts. Rapid historical spit elongation during the last 190 years has trapped an average of 681,000 m^3 yr^{-1} of sand; this occurred coincident with downdrift barrier-island erosion/migration at long-term rates of >3 m yr^{-1}. Historical sand fluxes to the elongating spit on southern Assateague Island and progradational beach ridges on northernmost Wallops Islands are equivalent to at least 60% of estimated regional longshore transport rates. We therefore propose that sediment trapping and associated wave refraction are the primary drivers of downdrift barrier erosion, while storminess and sea-level rise are secondary forcings of change affecting equally the entire barrier-island chain. Global context is provided by a compilation of sediment trapping through growth of similar longshore sand sinks, which indicates the volume of sediment incorporated into the elongating spit end of Assateague Island is similar to sandy beach- and foredune-ridge plains (10^8 m^3), but average annual trapping at the spit is at least six times greater than those at most mainland-attached, progradational systems. However, Chincoteague and Wallops, two progradational barrier islands, incorporate sand at rates broadly similar to large strandplains. Our findings emphasize the need to account for natural longshore sediment trapping in multi-decadal coastal management efforts on sandy, siliciclastic coasts.

1. Introduction

The interplay among accommodation, sediment supply, and myriad secondary factors such as antecedent geology, barrier-backbarrier couplings, and internal dynamics (*i.e.*, autogenic

* Corresponding author. PO Box 1346, Gloucester Pont, VA, 23062, USA.
E-mail address: jshawler@vims.edu (J.L. Shawler).

https://doi.org/10.1016/j.quascirev.2021.107096

processes) control the evolution of coastal barrier systems (*e.g.*, Belknap and Kraft, 1985; Walters et al., 2014; Hein et al., 2016; FitzGerald et al., 2018; Ciarletta et al., 2019a; Emery et al., 2019; Shawler et al., 2021). Coastal sediment fluxes to barrier islands are controlled by river sediment discharge (Hein et al., 2014a; Shawler et al., 2019a; Rodriguez et al., 2020), upstream and coastal human modifications (Syvitski et al., 2005; Laïbi et al., 2014), erosion and depletion of local sediment sources (Hequette and Ruz, 1991), and natural changes in cross- and longshore sediment fluxes (Otvos and Carter, 2013; Hollis et al., 2019). Accommodation creation is controlled by the interaction of inherited geology and relative sea-level change, including tectonics, subsidence, and eustatic sea-level change (Curray, 1964; Milne et al., 2009).

Sediment supply, defined here as variations in alongshore, cross-shore, and local fluxes of sediment (predominantly sand-sized) to barrier islands, can be influenced by various updrift and shoreface processes and sediment sources. In the cross-shore perspective, shoreface processes dictate sediment supply and time-varying barrier morphology (Cowell and Kinsela, 2018). Delayed interactions between wave erosion on the shoreface and barrier overwash can lead to periodic barrier-island retreat (Lorenzo-Trueba and Ashton, 2014) and cyclic deposition of sediments on the shelf (Ciarletta et al., 2019a). Cross-shore sediment supply is also controlled by the availability and magnitude of sediment sources constrained by framework geology such as paleovalleys, inlet fills, antecedent highs, and inner shelf sand volumes (*e.g.*, Wallace et al., 2010; Timmons et al., 2010; Wallace and Anderson, 2013; Anderson et al., 2016; Zaremba et al., 2016; Hapke et al., 2016; Hollis et al., 2019; Shawler et al., 2021; Gal et al., 2021). Alongshore controls on sediment fluxes and barrier and shoreline behavior include inlet processes and ebb-tidal delta bypassing (*e.g.,* FitzGerald, 1984; Fenster and Dolan, 1996; Van Heteren et al., 2006; Robin et al., 2020), shoreline hardening, artificial inlet stabilization and the construction of jetties and groins (*e.g.*, Hall and Pilkey, 1991; Garel et al., 2014; Hein et al., 2019a), headland bypassing (*e.g.*, Vieira da Silva et al., 2016a; Valiente et al., 2020; Oliver et al., 2020; Silva et al., 2021), erosion and/or reconfiguration of updrift sediment sources and sinks (*e.g.*, Ashton et al., 2016; Fruergaard et al., 2019; Torres et al., 2020), and changes in storminess and wave climate (*e.g.*, Fruergaard et al., 2013; Masselink and Van Heteren, 2014; Zăinescu et al., 2017). Additionally, sediment trapping by human and natural updrift features modifies coastal behavior at local (*e.g.*, Leatherman, 1979) to regional (*e.g.*, Ells and Murray, 2012; Hapke et al., 2013) spatial scales.

As demonstrated by these diverse studies, sediment trapping at groins, inlets, and ebb-tidal deltas is relatively well-understood. However, the role of the growth or erosion of natural updrift siliciclastic landforms, such as the filling of coastal embayments, erosion of sandy headlands, and progradation/elongation of barrier islands/spits remains understudied (see Hein and Ashton, 2020). Specifically, the formation and collapse of updrift sediment sinks can regulate downdrift sediment fluxes and play a predominant role in the behavior of sandy coastal landforms (Anthony, 1995, 2015; Park and Wells, 2007; Fruergaard et al., 2019, 2021, ; Oliver et al., 2020), but the dynamics, volumes, and fluxes of sediment trapped and mobilized are poorly constrained.

What are the magnitudes of sediment trapping at progradational barrier islands and elongational spits and what are associated effects on longshore transport and the behavior of the downdrift coast? To answer this question we integrate millennial, centennial, and decadal records of sediment fluxes trapped in the progradational-elongational Assateague-Chincoteague-Wallops barrier-island system (northern Virginia, USA; Fig. 1) to reconstruct the multi-kilometer-scale development and morphodynamics of this sandy coastal sediment sink. Additionally, we integrate geospatial, sedimentological, and geochronological data to calculate volumetric storage and explore the drivers of time-varying fluxes of sediment trapped in the system. We place sediment storage at this site in context with other potential drivers of downdrift coastal erosion including sea-level rise, increased storm frequency, variations in framework geology, and an alongshore transport gradient. Finally, we compare the sediment stored in this system to estimates of sediment stored in similar globally distributed coastal depositional landforms to ascertain the global applicability of these findings.

2. Regional setting

2.1. Coastal setting

The Assateague-Chincoteague-Wallops barrier-island system is located on the central U.S. mid-Atlantic coast, surrounding the north-south-oriented Chincoteague Inlet (Fig. 1). Landward of these barriers is the Virginia portion of the Delmarva Peninsula, composed of unconsolidated coastal plain sediments deposited during at least five interglacial highstands (Krantz et al., 2016). The Assateague-Chincoteague-Wallops system is situated at the north-to-south transition from long, linear wave-dominated barrier islands of southern Delaware and Maryland, to the shorter, mixed-energy Virginia Barrier Islands. Tropical and extratropical cyclones drive the southerly regional sediment transport system (Fenster et al., 2016). Regional extratropical cyclone frequency has increased from the late 1800s−1990s (Hayden and Hayden, 2003) and hurricane-generated wave heights have increased since the 1970s (Komar and Allan, 2008). Based on records from 1978 to 2015 CE, two local tide gauges record mean tidal ranges of 1.23 m (Wachapreague, VA; 30 km south of the study site) and 0.64 m (Ocean City, MD; 50 km north of the study site; Fenster and McBride, 2015). Local wave data from 1980 to 2012 CE indicate dominant wave heights of 1.2 m and mean wave periods of 8.3 s near Assateague Island (Fenster and McBride, 2015).

Chincoteague Inlet, which separates southern Assateague Island and northern Wallops Island has an approximately north-south orientation and conveys water and sediment between the Atlantic Ocean and the southern portion of Chincoteague Bay and the northern backbarrier lagoon of Wallops Island (Beudin et al., 2017). The inlet is approximately 1.8 km wide, with an 8−12 m deep main channel located on the western margin of the inlet and a shallow (~2 m deep) platform/shoal located to the east of the main channel (McPherran et al., 2021). The inlet has a mean tidal range of 0.66 m, average significant wave height of 1.11 m, and a 44 million m^3 tidal prism (Jarrett, 1976). During strong wind events, changes in wind direction and intensity drive exchange between Chincoteague Bay and the Atlantic Ocean; during weak wind events, tidal forcing dominates exchange processes (Kang et al., 2017). For example, inflow to Chincoteague Bay through Chincoteague Inlet increases during periods of strong southwest winds, while outflow increases with northwesterly winds (Kang et al., 2017). Following major storms, freshwater exits Chincoteague Bay through the inlet, with velocities capable of mobilizing sediment (McPherran et al., 2021).

2.2. Morphology of Assateague, Chincoteague, and Wallops islands

The present-day morphologies of the Assateague-Chincoteague-Wallops barrier-island system attest to the spatial and temporal complexity of processes operating along this reach. Despite this complexity, the presence of beach-and foredune-ridge plains across islands provides a means for unraveling the

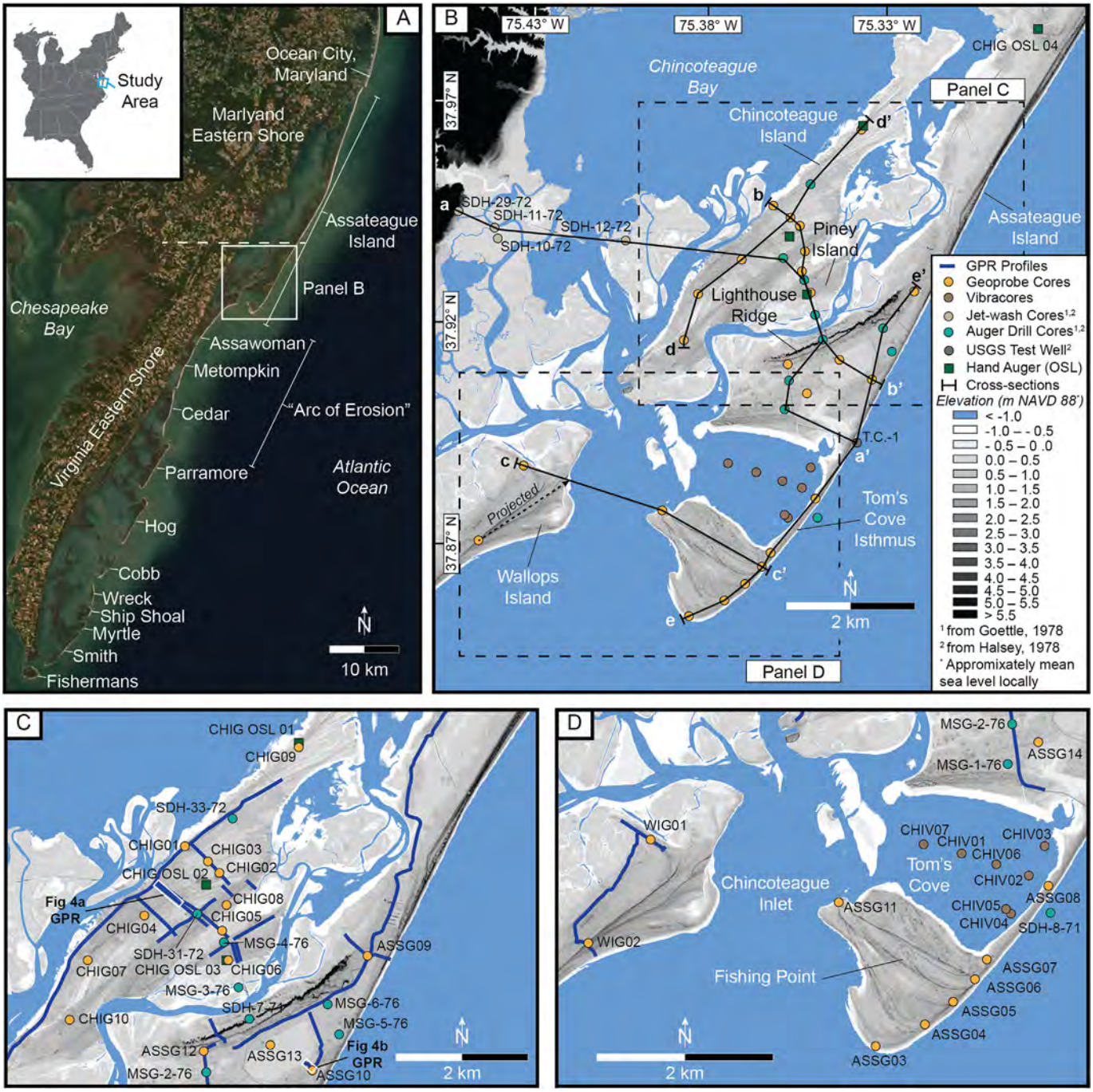

Fig. 1. Study area and field data collected from the Assateague-Chincoteague-Wallops barrier-island system A) The southern Maryland and northern Virginia barrier-island coast. Assateague Island is ~58 km long, with the southern terminus consisting of progradational beach-and-foredune ridges. South (downdrift) of southern Assateague is a shoreline offset, described locally as an "arc of erosion". Imagery from Esri. B) Study site showing locations of ~34 km of ground-penetrating radar tracklines, 24 direct-push Geoprobe (~20–24 m long) cores (this study), 15 auger and hydrologic test drill cores (Halsey, 1978; Goettle, 1978), seven vibracores (0.6–5 m long; this study), optically stimulated luminescence sampling sites (hand augers; this study), and primary stratigraphic cross-sections. C and D) Panels show additional detail and core labels. Where human disturbance is minimal, distinct ridge and swale topography is evident on Chincoteague, Assateague, and Wallops islands. The southern terminus of Assateague is marked by curvilinear beach and foredune ridge features formed by spit elongation. DEM from lidar (USGS, 2016).

evolutionary history of this region, determining barrier-system morphodynamics, and inferring causative mechanisms for individual landform formation.

At 58 km in length, the wave-dominated Assateague Island is among the longest islands on the U.S. East Coast. The series of recurves which comprise the southern portion of the island are marked by variably-oriented beach and foredune ridges (generally 1–3 m high; Fig. 2). The tallest such ridge ("Lighthouse Ridge") exceeds 8 m in height and is the location of the *ca.* 1830 CE shoreline, where a coastal navigation light was originally constructed in 1833 CE. Since around 1830 CE the island has elongated to the south nearly 7 km as multiple beach- and foredune-ridge sets, including "Fishing Point" (or "Tom's Cove Hook") joined to Assateague proper by the narrow (~500 m wide) Tom's Cove

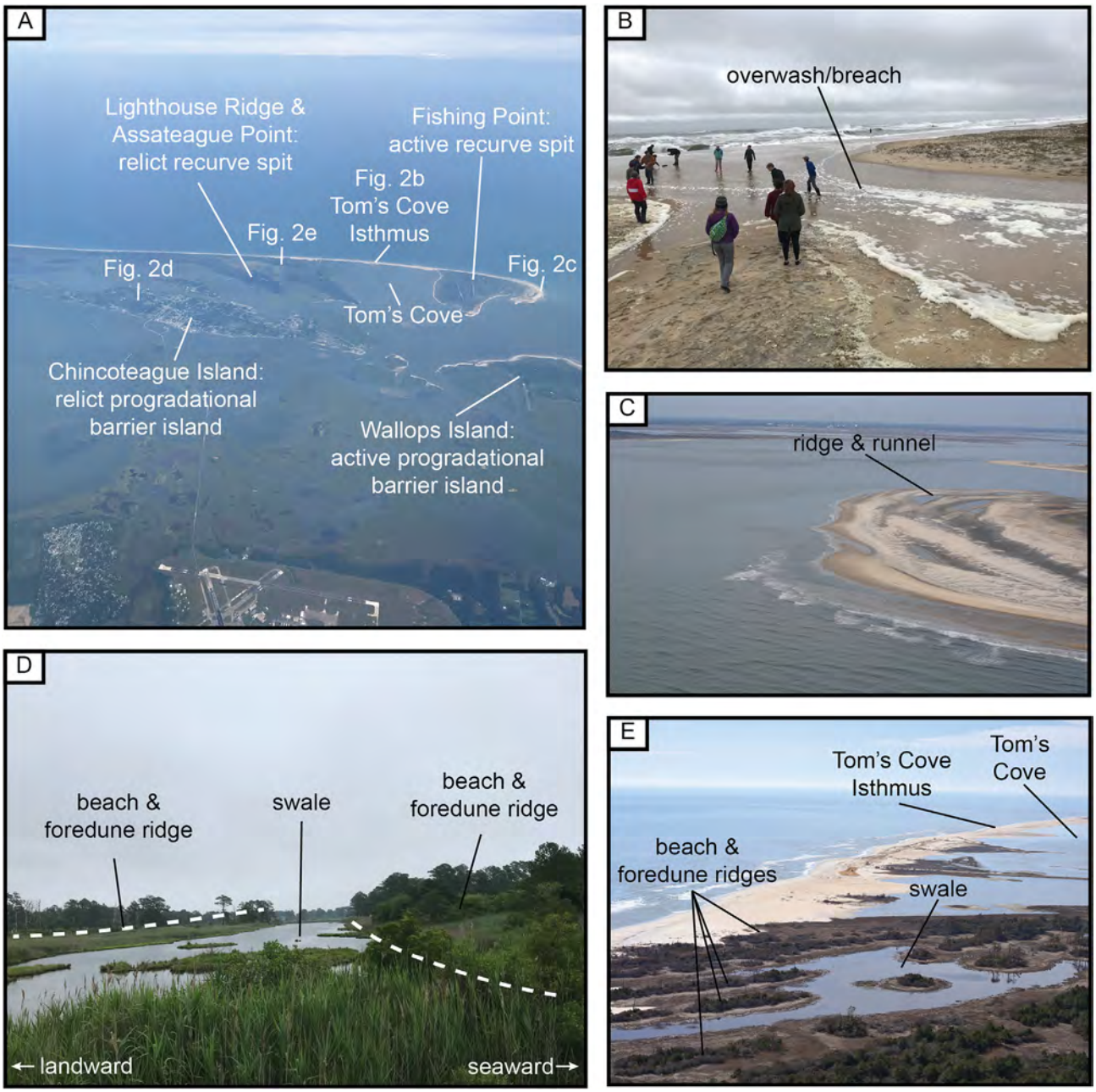

Fig. 2. Photographs of morphological features and depositional environments on Assateague, Chincoteague, and Wallops islands (Virginia, USA). A) Aerial photo highlighting the morphology of the relict and modern depositional environments in the study area. Additional labels correspond to subpanels of this figure. Credit: J. Shawler. B) An ephemeral breach with active overwash transport occurring during a non-tropical storm event on October 27, 2018. Credit: J. Shawler. C) Ridge and runnels forming on the active portion of the recurved spit end of Assateague Island, Virginia. Credit: USGS Public Domain. Taken on March 8, 2016. D) Ridge and swale topography on Chincoteague Island, a relict progradational barrier island. Credit: J. Shawler. E) Ridge and swale topography on the relict recurved spit of Assateague Island. Ridges are oriented sub-parallel to the modern shoreline. Credit: USGS Public Domain.

Isthmus. The southern spit-end grew at a long-term (1800s–2000) rate of 21.5 m yr^{-1} and an average near-term (1970–2000) rate of 40.3 m yr^{-1} (Hapke et al., 2010). The overall system morphodynamics are more complicated and include areas of erosion and variable alongshore progradation rates (Hein et al., 2019b). Today, the U.S. Fish and Wildlife Service manages the southern portion of the island as a wildlife refuge with light recreational uses permitted. Because of the interruption of longshore sediment transport by the Ocean City Inlet jetties to the north, the northernmost ~10 km of Assateague Island (located > 40+ km from our study site) has been nourished four times since 1998 CE (Campbell and Benedet, 2006; ASBPA, 2020; Elko et al., 2021). By contrast, Ocean City, Maryland—located immediately north of Assateague and Ocean City Inlet —has been nourished fourteen times since 1963 CE with seven of those nourishment projects occurring since 1998 CE (Campbell and Benedet, 2006; ASBPA, 2020; Elko et al., 2021).

Chincoteague Island, today located entirely landward of Assateague Island, was once an open-ocean barrier. The Pocomoke Native Americans originally hunted and fished on the island, which was later occupied by Europeans beginning in the mid-17th century. Eventually, Chincoteague evolved into a fishing village by the

late 19th century, and today houses a growing tourist economy. A series of variably oriented (WSW-ENE and SW-NE) arcuate beach and foredune ridges (<1–2 m high) exist on Chincoteague Inlet in areas undisturbed by development (Figs. 1 and 2). The island varies in width from ~500 to 1500+ m. Immediately to the east, Chincoteague is fronted by Piney Island, which is either a former part of Chincoteague Island or a separated recurve of Assateague Island (see Goettle, 1978).

South and west of Chincoteague Inlet, the more than 15 km long Wallops Island possesses a bulbous northern end (~1500 m wide) and progressively narrower (~300 m wide) southern terminus. The northernmost end contains a series of arcuate beach and foredune ridges oriented SW-NE, most of which formed during the late 20th and early 21st centuries. An inlet separating Wallops Island from Assawoman Island (immediately to the south) closed in the mid-1980s in response to an engineered reduction in tidal prism (Fenster and Bundick, 2015). Since 1945 CE, the National Advisory Committee for Aeronautics and its successor, the National Aeronautics and Space Administration (NASA), has owned and managed Wallops Island. Consequently, the majority of Wallops Island has experienced heavy engineering and human alterations, including most recently construction of a seawall, multiple episodes of beach nourishment (years: 2012 CE, 2014 CE [Fenster and Bundick, 2015]), and the in-progress (2021 CE) construction of shore-attached breakwaters backfilled with sediment removed from the northern end of the island. The need to protect infrastructure from the complex hydrodynamic and sediment transport processes at Chincoteague Inlet and the refraction of waves around the southernmost portion of Assateague Island drives the human management of this system. This wave refraction creates a nodal zone which moves sand both southward and northward at a maximum flux of ~46,000 m^3 yr^{-1} (King et al., 2011), and feeds the rapidly growing northern end of the island (up to 16 m yr^{-1}; Hapke et al., 2010). The sediment transported to the south of this nodal zone plays a major role in supplying the southern Virginia Barrier Islands with beach-quality sand. However, modeling results (Generalized Model for Simulating Shoreline Change) indicate that net sediment transport fluxes decrease rapidly to the south from the nodal point and that the southerly flux gradients correspond closely with shoreline retreat rates (King et al., 2011).

2.3. Holocene development and sea-level history

The Holocene age barrier-backbarrier systems along the Virginia and Maryland coasts developed atop Pleistocene-aged estuarine sediments, likely deposited during Marine Isotope Stage 5 (Goettle, 1978). The Holocene system consists of silty lagoonal deposits and sandy marine shoal/shoreface, barrier, and dune-ridge sediments (Goettle, 1978). Using 12 auger borings, three uncalibrated radiocarbon dates, and three amino acid racemization age estimates, Goettle (1978) proposed that the Assateague-Chincoteague-Wallops barrier system developed first with Chincoteague Island as an open-ocean barrier *ca*. 2000 years ago, followed by southerly growth of Assateague Island seaward of Chincoteague in a series of seven distinct phases, as exemplified by the development of associated ridgesets. Seminack and McBride (2015a) refined the model to incorporate the opening and closure of multiple inlets along the entire ~58 km length of Assateague.

Relative sea level on the Virginia coast rose 8.5 m over the last 5000 years, at an average rate of ~1.5 mm yr^{-1} between 5000 and 4000 years ago until it slowed moderately to ~1.3 mm yr^{-1} from 4000 years ago to 1900 CE (Engelhart and Horton, 2012). Preservation of backbarrier deposits and the development of the Holocene barrier-island system along the Virginia coast coincided with this rise in sea level over the middle to late Holocene (Finklestein and Ferland, 1987; Raff et al., 2018). Over the late 20th century to present, regional sea level rose at a rate of 3.5–5 mm yr^{-1} (Boon and Mitchell, 2015).

3. Methods

3.1. Paleo-shoreline mapping

Historical shoreline-change data from southern Assateague Island are derived from Hein et al. (2019b). We mapped pre-historical shoreline positions from beach and foredune ridge morphology using modern satellite imagery and USGS (2016) topobathy lidar. We obtained additional geochronology from either historical records (georeferenced historical maps and NOAA t-sheets) or optically stimulated luminescence (OSL) dating.

We collected four samples for OSL analysis from wave-built lithofacies using methods described by Oliver et al. (2015). These were analyzed at the OSL dating laboratory at the University of Illinois, Urbana-Champaign (Table 2). The PVC pipe cores were opened, and the mineral extraction was conducted in a subdued orange light environment. Ten centimeters of sediment was removed from the bottom (to avoid any sediment unintentionally exposed to sunlight during collection). The actual OSL sample was extracted about 15 cm from the bottom of the core and treated with 10% hydrochloric acid (HCl) and 20% hydrogen peroxide (H_2O_2) to remove carbonate and organic material. The sediment was then dried and sieved to separate grains in the ~2.7–2.0 phi size range (150–250 μm). Quartz grains from these samples were extracted and none showed any significant contamination from feldspar. For the equivalent dose (De) measurements, we relied on an automated Lexsyg Smart system (Richter et al., 2015), and measurements were carried out with a single-aliquot regenerative dose (SAR) protocol (Murray and Wintle, 2000, 2003). To obtain the dose rate, sediments from the bottom section of each core were dried, a representative portion was encapsulated in petri dishes (~20 g) and sealed with two coatings of epoxy gel. The specific activities (Bq/kg) were measured with a broad-energy high-purity germanium (BEGe) detector, in a planar configuration. Further details can be found in the supplementary materials.

3.2. Ground-penetrating radar

A total of ~34 km of predominantly cross-shore and shore-parallel ground-penetrating radar (GPR) surveys were conducted across all three islands using a 250 MHz MALA Geosciences shielded antenna. GPR lines were topographically corrected using elevation profiles derived from USGS (2016) topobathy lidar. All GPR data were post-processed following the methods of Carruthers et al. (2013) using site-specific filtering, migration, and variable gain control and time-depth converted using a migration-derived radar velocity of 7 cm/ns using DECO-Geophysical Co. Ltd.'s RadExplorer software program. The radar velocity value was selected from established values for saturated sandy barrier sediments (*e.g.,* Oliver et al., 2019a) given the presence of a shallow (<50 cm) fresh groundwater table at all sites.

3.3. Onshore and offshore stratigraphy

We collected 24 direct-push (Geoprobe) sediment cores (20–24 m deep) across all three islands (Fig. 1) to characterize their pre-Holocene and Holocene stratigraphy. Additionally, we collected seven vibracores (0.6–5 m deep) in Tom's Cove, the shallow lagoon landward of the southern Assateague isthmus. All cores were

opened, photographed, and described using visual standards for sediment grain size, texture, mineralogy, and color (Munsell). Grain-size distributions of select core samples (based on facies descriptions) were determined using a Beckman-Coulter Laser Diffraction Particle Size Analyzer. Samples were run in triplicate, and data are reported as averages of the triplicates. Geochronological control of stratigraphic layers is provided by radiocarbon samples from various depths in direct-push cores. Accelerator mass spectrometer radiocarbon analyses of 11 shell, peat, and terrestrial root samples were performed at the National Ocean Sciences Accelerator Mass Spectrometry Facility (NOSAMS; Woods Hole, MA, USA). All radiocarbon ages, including two additional ages from prior work (Halsey, 1978; Goettle, 1978), were calibrated using OxCal 4.4 (Bronk Ramsey, 2009), which includes a reservoir correction. Terrestrial samples (peat, roots) were calibrated with Intcal20 (Reimer et al., 2020) calibration curves and marine samples (all mollusks) were calibrated using Marine20 (Heaton et al., 2020), corrected to a ΔR of −33 ± 40 years (Rick et al., 2012).

To investigate the offshore stratigraphy and characterize the mobile shoreface sediments, 38 km of high-resolution (submeter) seismic data were collected at ~0.5–1.0 km line spacings using an Applied Acoustics AA300 boomer (operated between 150 and 300 J) seismic system with a CSP300 seismic energy source and 4.5 m long Applied Acoustics hydrophone streamer with 8 elements. A Trimble DSM 132 dGPS marine positioning receiver and antenna enabled merging real-time digital geographic positions to digital SEG-Y seismic data. This system provided submeter horizontal positional accuracy and up to 60 m of penetration based on an assumed sound velocity of 1500 m/s. Chesapeake Technologies' SonarWiz software version 7 was used for data acquisition, processing, and interpretation. Seismic facies were interpreted based on a seismic facies analysis (Sangree and Widmier, 1979) and seismic facies correlation with previous studies from this same region (*e.g.*, Toscano et al., 1989; Wikel, 2008; Brothers et al., 2020).

3.4. Sediment volumes and fluxes

Sediment volumes were determined for Assateague, Chincoteague, and Wallops islands by multiplying the area of each island by an average thickness of the barrier island. Modern areas were mapped using recent basemap imagery in ArcGIS 10.6 (Esri) and historical areas were mapped using shoreline and area data compiled from previous publications (*e.g.*, Deaton et al., 2017; Hein et al., 2019b) and additional historical maps and charts. To calculate barrier thickness, the average height of undisturbed ridges and swales above North American Vertical Datum of 1988 (NAVD 88) was measured on each island from a high-resolution lidar DEM and an estimated average depth below NAVD 88 was determined from sediment cores. For each paleo-shoreline a conservative estimate of foreshore volume of was calculated by multiplying the shoreline distance by the area of a simplified right-triangle-shaped wedge of foreshore sand. Estimates of foreshore maximum thickness (5.5 m Assateague, 5.3 m Chincoteague, 6.5 m Fishing Point, and ~3 m Wallops) and cross-shore length (75 m for all) were determined from modern foreshore bathymetry (USGS, 2016) and are consistent with sediment core data from this study. We acknowledge that a singular thickness value for the barrier and foreshore does not capture potential variability in ridge and swale topography or in subaqueous depth, but, by far, the largest factors controlling island volume estimates are island area and shoreline length, respectively. Fluxes were calculated by dividing total barrier and foreshore volumes by the period of deposition. Additionally, volumetric estimates of mixed mud and sand shoreface deposits were calculated using the same approach.

4. Results

4.1. Shoreline geochronology and progradation

A combined dataset of OSL dates (Table 1; Fig. 3) and historical shoreline data (Fig. 3) provide geochronological control for the physical evolution of Assateague, Chincoteague, and Wallops islands. The westernmost ridge on Chincoteague Island formed *ca.* 2250 years ago, while the eastern-most ridge formed *ca.* 400 years ago (~1620 CE; Fig. 3; Table 1). An OSL date from a ridge on Assateague Island, at the northernmost limit of our study site, returns an age of *ca.* 120 years ago (~1900 CE), approximately coincident with the closing of an updrift inlet (Seminack and McBride, 2015) and, to the south, growth of Lighthouse Ridge adjacent to the *ca.* 1830 CE shoreline.

Assateague Island prograded in a generally southeast direction from 1830 CE to 1859 CE but began a south to southwesterly elongation in the late 1800s, which has continued to present (Fig. 3). The northern end of Wallops Island prograded in a net easterly to northeasterly direction between the late 1800s and present. Central Wallops largely eroded or remained stable during that same period (Fig. 3).

Shoreline progradation is evident not only in historical maps, but also in GPR profiles from Chincoteague and central Assateague islands (Fig. 4). On Chincoteague, a combination of seaward-dipping (~1.5–3.0°) subsurface reflections imaged in radar profiles and ridge ages that are progressively younger to the east indicate that the island built seaward from *ca.* 2250 to *ca.* 400 years ago. A similar set of observations from Assateague Island, albeit with a much younger set of shorelines (1830 CE to present), likewise reveals the progradational development of that system.

4.2. Stratigraphic units and interpretations

Sedimentological data (Figs. 5–7), radiocarbon dates (Table 2), and seismic facies and interpretations (Fig. 8) together inform the primary stratigraphic units within the Assateague-Chincoteague-Wallops barrier-island system and the proximal offshore region (Tables 3 and 4). Seismic facies interpretations and seismic unit identification are based on newly obtained nearshore seismic data, ground-truthed with onshore sediment cores obtained in this study and correlated to existing offshore seismic data of Brothers et al. (2020).

4.2.1. Pleistocene shallow marine

The lowermost unit is composed of a shelly, glauconitic, greenish-gray (Munsell color: Gley 1 5GY 5/1) sandy clay to silty or clayey very fine sand (median grain size: 0.02–0.19 mm; Table 3). The clay content is highly variable (sorting: 3φ) and shell hash is abundant within this facies. This unit is encountered in cores from Chincoteague Island and the central and northern portion of the study site on Assateague Island (depth: −15 m MSL and deeper) but was not observed underlying Wallops Island and Fishing Point.

This facies most likely formed in a shallow marine depositional environment. Radiocarbon dates (one >45,000 calibrated years before present [cal. Yrs BP]) located stratigraphically above this unit indicate a Pleistocene or later age for this unit. Goettle (1978) interpreted this unit as being the mouth of an estuary or an inlet possibly built during one or more sea-level highstands.

The equivalent seismic unit is characterized by both gently seaward (0.4–0.9°) and southerly (0.06–0.15°) dipping reflections but is reflection free in places (Fig. 8). The unit is likely equivalent to unit Qpp observed and described by Brothers et al. (2020) as a Pleistocene transgressive system tract which fills the Persimmon Point paleochannel (active during Marine Isotope Stage 22, 16, or

Table 1
Optically stimulated luminescence (OSL) dates.

Sample	ISGS code	depth (m)	U ($^{226}Ra)_{eq}$ (ppm)	Th (ppm)	K (%)	Equivalent dose (Gy)	Dose rate (Gy/ka)	Age (ka)	n (accepted/total)
ASSGOSL01	701	1.400	2.20 ± 0.02	6.18 ± 0.11	0.610 ± 0.016	0.166 ± 0.009	1.43 ± 0.05	**0.116 ± 0.008**	74/270
CHIGOSL01	702	1.285	0.742 ± 0.014	1.95 ± 0.04	0.485 ± 0.012	1.96 ± 0.04	0.87 ± 0.03	**2.25 ± 0.10**	77/200
CHIGOSL02	703	1.285	0.544 ± 0.020	1.44 ± 0.05	0.74 ± 0.02	1.23 ± 0.03	0.97 ± 0.04	**1.27 ± 0.07**	39/111
CHIGOSL03	704	1.240	0.441 ± 0.017	1.55 ± 0.05	1.34 ± 0.03	0.56 ± 0.02	1.38 ± 0.06	**0.40 ± 0.02**	36/125

Table 2
Radiocarbon dates.

Sample ID	NOSAMS accession #	Latitude	Longitude	Sample Elevation (m NAVD 88)	Stratigraphic Unit	Dated Material	Reported Age (^{14}C yrs BP)	δ^{13}C (‰ VPDB)	Cal. 2-σ age (yrs BP)	Probability (%)
CHIG05 Drive 10 60.5–64.5 cm	OS-155379	37.92852	−75.35656	−10.86	transitional gyttja/peat	saltwater peat	5380 ± 30	−14.55	**6228 ± 55** 6131 ± 18 6029 ± 20 6069 ± 9	**66** 17.2 9.4 2.9
CHIG05 Drive 10 85–86 cm	OS-155342	37.92852	−75.35656	−11.10	Pleistocene estuarine	*Mulinia lateralis*	41,800 ± 2400	0.92	**45,108 ± 2970**	**95.4**
ASSG09 Drive 10 30–31 cm	OS-155344	37.92406	−75.32453	−10.24	Holocene shoreface	*Mulinia lateralis*	1940 ± 20	1.44	**1368 ± 75**	**95.4**
CHIG01 Drive 08 73.5–75 cm	OS-155345	37.94326	−75.36481	−8.50	Holocene backbarrier	*Urosalpinx cinerea*	4300 ± 25	−0.12	**4273 ± 99**	**95.4**
ASSG08 Drive 09 9–10 cm	OS-155346	37.87719	−75.35253	−8.65	Holocene shoreface	*Mulinia lateralis*	575 ± 15	0.2	**53 to modern**	**95.4**
ASSG08 Drive 10 90–91 cm	OS-155347	37.87719	−75.35253	−10.68	Holocene shoreface	*Mulinia lateralis*	780 ± 20	0.83	**276 ± 88**	**95.4**
ASSG06 Drive 10 80.5 −81.5 cm	OS-155348	37.86178	−75.36768	−10.09	Holocene shoreface	*Mulinia lateralis*	610 ± 20	0.75	**106 ± 74**	**95.4**
WIG02 Drive 08 76–77 cm	OS-155349	37.86740	−75.44846	−6.41	Holocene backbarrier	*Urosalpinx cinerea*	2860 ± 20	1.88	**2483 ± 97**	**95.4**
ASSG11 Drive 11 45.5 −47.5 cm	OS-155350	37.87432	−75.39611	−11.52	Holocene backbarrier	*Urosalpinx cinerea*	2650 ± 25	1.84	**2210 ± 89**	**95.4**
ASSG03 Drive 10 25–26 cm	OS-155351	37.85052	−75.38839	−10.27	Holocene shoreface	*Mulinia lateralis*	550 ± 15	0.04	**36 to modern**	**95.4**
CHIG08 Drive 11 53–57 cm	OS-155272	37.93295	−75.35570	−12.00	transitional gyttja/peat	Terrestrial plant stem/ root	5620 ± 30	−29.72	**6382 ± 72** 6476 ± **7**	**92.3** 3.1
MSG-6-76 (Goettle, 1978)	N/A	37.91567	−75.33333	−11.88	Pleistocene estuarine	wood fragments	25,860 ± 660	N/A	**30,143 ± 641**	**95.4**
SDH-33-72 (Halsey, 1978)	N/A	37.94817	−75.35417	−10.36	transitional gyttja/peat	peat	28,700 ± 850	N/A	**33,027 ± 953**	**95.4**

^{14}C ages were calibrated using OxCal 4.4 (Bronk Ramsey, 2009), which includes a reservoir correction. Terrestrial samples (peat, roots) were calibrated with Intcal20 (Reimer et al., 2020) calibration curves and marine samples (all mollusks) were calibrated using Marine20 (Heaton et al., 2020), corrected to a ΔR of −33 ± 40 years (Assateague Island backbarrier value from Rick et al., 2012).
All dates in text are reported as 2-sigma median calibrated ages before 1950 (in bold) with error derived from full range of possible calibrated ages and incorporating instrument error.

12; Table 4). This interpretation is consistent with the seaward and southerly dipping to absent internal reflections seen in our seismic data and the likely marine origin indicated by our sediment-core data.

4.2.2. Pleistocene estuarine

A fining-upward facies (~−10 to −15 m MSL) directly overlies the lower-most unit observed in these cores. Under Wallops and Chincoteague islands, this is the deepest unit observed (Figs. 6 and 7). This unit transitions from a basal coarse sand with pebbles, some shell fragments, and some whole shells to a laminated silty clay and very fine sand. The upper portion of the unit alternates between sections of flaser and lenticular bedding (average sorting: ~2φ) (Table 3). The coarse-grained basal section contains abundant pebbles (>2 mm); the finer than 2 mm subsample has a median grain size of 0.25 mm. The finer-grained uppermost section has a median grain size of 0.01–0.20 mm. Color ranges from a grayish brown (coarse section; Munsell color: 10 YR 5/2) to dark gray (fine section; Gley 1 4/N).

Mottling and oxidation at the topmost unit (*i.e.*, evidence of possible subaerial exposure) as well as an "infinite" radiocarbon age (>45,000 cal Yrs BP) of a sample from the top of this unit indicate a Pleistocene age for the facies. Therefore, we interpret this unit as representing a Pleistocene estuary which transitions up-section from greater terrestrial/fluvial influence (coarse grained) to more marine/tidal influence (fine grained; laminated).

The corresponding seismic unit is low-amplitude to reflection-free (Fig. 8; Table 4). The base of the seismic unit is a high-amplitude, continuous gently-seaward-dipping (0.03–0.05°) to planar (*i.e.*, 'flat') reflection at a depth of 15–20 m below MSL (Fig. 8; Table 4). This seismic facies corresponds to the Q2 unit described by Brothers et al. (2020) as a highstand systems tract of estuarine and marine origin, while the lower contact of the unit corresponds to the Pleistocene-age U7 unconformity (transgressive

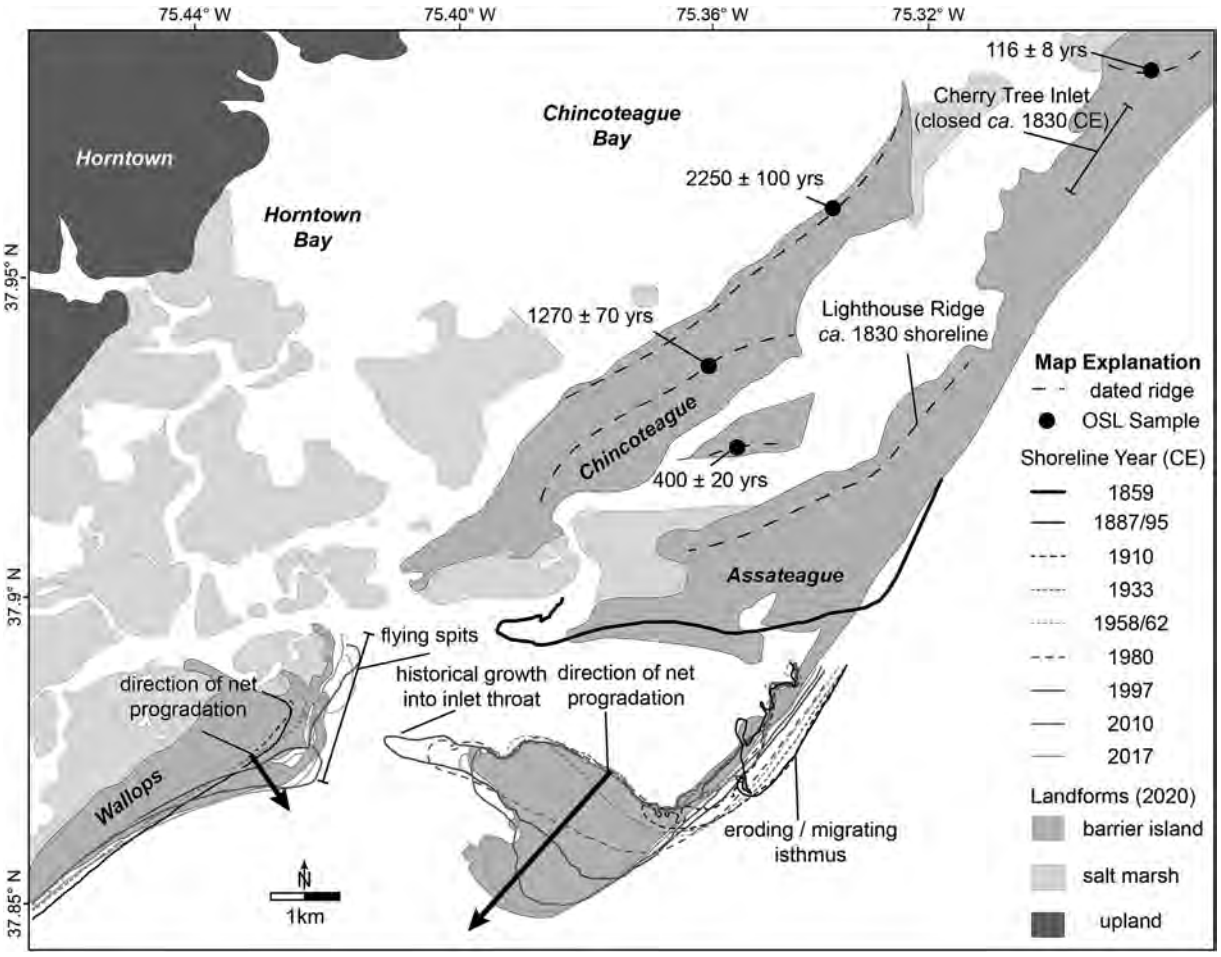

Fig. 3. Compilation of shoreline chronology from optically stimulated luminescence (OSL) dating, historical references (inlets, Lighthouse Ridge), and a timeseries of shoreline data from charts and aerial images. OSL data indicate Chincoteague Island began widening *ca.* 2250 years ago, with the youngest dated shoreline forming *ca.* 400 years ago. Lighthouse Ridge on Assateague Island approximates the location of the 1830 CE shoreline. Since the 1800s, Assateague Island has prograded dominantly to the south through a series of recurved spit ridges, while the northern end of Wallops Island has prograded dominantly from the west to the east. Only select shorelines are shown.

ravinement surface) which truncates the underlying Pleistocene shallow marine unit (Qpp; Brothers et al., 2020).

4.2.3. Transitional peat/gyttja/soil

Situated stratigraphically above the fining-upward unit is a black to very dark grayish brown (Munsell colors: 10 YR 2/1 and 10 YR 3/2) organic-rich silty soil to peat up to 50 cm thick, but typically observed as <25 cm thick with a median grain size of ~0.035 mm (Table 3). This unit is laterally discontinuous from the mainland to the ocean on Chincoteague Island and in the central and northern portions of our Assateague Island study area (Fig. 6a). It is entirely absent in the cores from Wallops Island and Fishing Point (Fig. 6b). Radiocarbon ages of samples from the top (6400–6200 cal Yrs BP) and the bottom (>45,000 cal Yrs. BP) of this unit indicate that it is likely a transitional peat or gyttja formed at the leading edge of Holocene transgression.

4.2.4. Holocene lagoon

This unit, which unconformably overlies the transitional and/or Pleistocene deposits under Chincoteague and Wallops islands and landward of the isthmus on southern Assateague, is composed of dark gray (Munsell color: 10 YR 4/1) clayey silt to silty clay with very fine sand lenses; snail shells (*Urosalpinx cinereal*) and shell hash are rarely observed (Table 3). The median grain size of samples from this facies ranges from 0.01 to 0.03 mm and sorting is ~2φ. In Tom's Cove (landward of the narrow isthmus on southern Assateague) a series of shallow (0.6–5 m) vibracores reveal the uppermost stratigraphy of this unit (see Fig. 1 for locations). Proximal to the isthmus, the sediment is dominantly fine to medium sand with lenses of silt, silty sand, and/or coarse sand. Distal from the isthmus, towards the center of the cove, the sediment is dominantly clayey silt with lenses of very fine to fine sand (−5.2 to −2.5 m msl), while towards the modern inlet (western portion of Tom's Cove) the sediment in this unit coarsens upward from clayey silt (−5 to −3.5 m MSL) to silty sand and sandy silt (−3.5 to −2 m MSL). Halsey (1978) observed this unit landward of Chincoteague Island, where it is up to 10 m thick and contains saltmarsh peat in the uppermost meter (Fig. 5). The unit is up to 5 m thick underlying the landward-most portions of Chincoteague and Wallops islands but thins seaward and disappears entirely under easternmost Chincoteague and central Fishing Point (Fig. 6).

Radiocarbon dates of samples collected from within this unit (4300–2200 cal Yrs. BP) and at its base (6400–6200 cal Yrs. BP) indicate a middle Holocene to modern age. Thus, we interpret the sediments in this unit as deposited in a Holocene backbarrier lagoon, with the uppermost portions of this unit landward of modern Chincoteague, Wallops, and Tom's Cove Isthmus continuing to accumulate sediment to the present time.

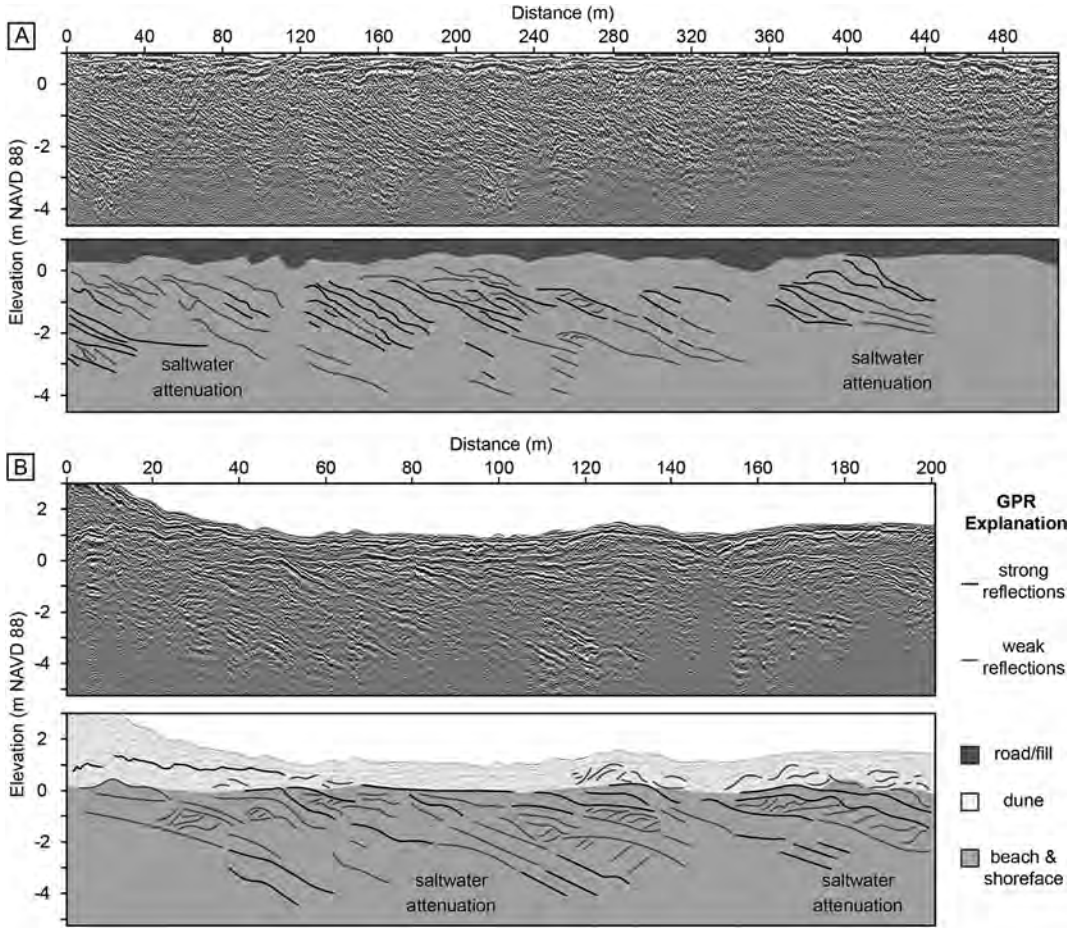

Fig. 4. Evidence of seaward progradation revealed by processed (top) and interpreted (bottom) ground-penetrating radar lines from A) Chincoteague Island and B) Assateague Island. In each line both strong and weak reflections are interpreted and used to distinguish between primary radar units. See Fig. 1 for locations. Profile A was collected across a flat road whereas the surface of Profile B tracks the complex ridge-swale morphology of south-central Assateague Island.

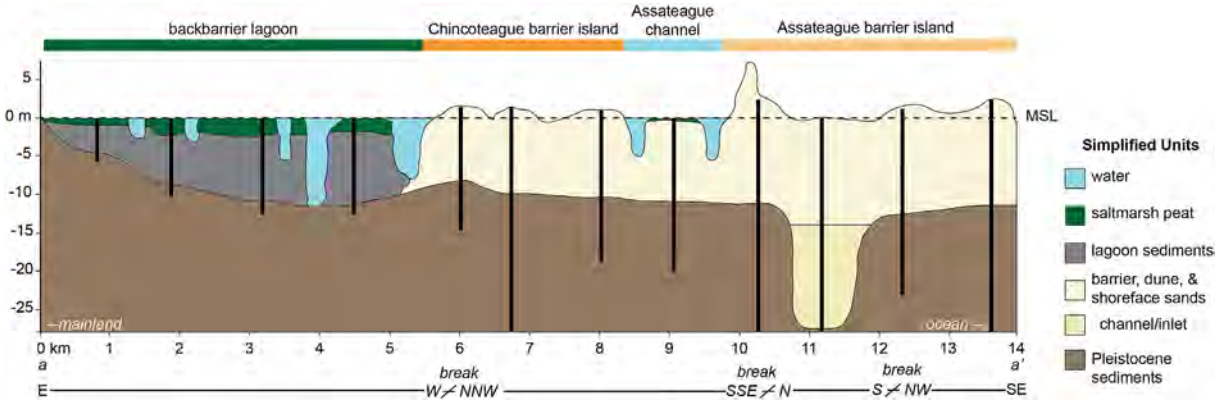

Fig. 5. Simplified stratigraphic cross-section a-a' (see Fig. 1 for location), modified from Halsey (1978). Backbarrier lagoon and saltmarsh sediments (together up to 10 m thick) are located landward of Chincoteague Island, a relict progradational barrier island. Assateague Island, an elongational barrier island/spit, is located seaward of Chincoteague Island. Note multiple changes in orientation given by the "breaks" along the profile.

4.2.5. Holocene shoreface and foreshore

Overlying and seaward of the dominantly muddy Holocene lagoon is a heterogenous mixed sand and mud unit. Specifically, this unit contains gray (Munsell color: 10 YR 5/1) dominantly fine to very fine sand (median grain size: 0.11–0.30 mm) with some sandy silt, lenses of pure silt and rarely observed clay with abundant dwarf clam shells (*Mulinia lateralis*) and shell hash (Table 3). The unit generally coarsens upward from muddy very fine sand to muddy to clean fine sand in all cores. Samples from the facies are moderately to poorly sorted (average sorting: 0.9φ). However, the unit is laterally variable with the shallowest (−5 m MSL or shallower) and thinnest deposits (3 m or less) observed on westernmost Chincoteague and northern Wallops Island, and the deepest (−15 m MSL) and thickest (6–7 m) observed under Fishing Point/

Table 3
Stratigraphic units.

Unit	Description	Depth Range (m MSL)	Depositional Environment
Pleistocene shallow marine	shell-rich sandy clay, clayey-sand and silty sand; abundant shell fragments with few whole shells; possibly glauconitic	−15 to - 24 and likely deeper	inner shelf
Pleistocene estuarine	dominantly laminated clay and fine silty sand; coarse sand and pebbles in deepest sections; occasional dwarf clams (*Mulinia lateralis*), partial oyster shells (*Crassostrea virginica*), and unidentifiable shell hash	−10 to −15	estuarine
Transitional peat/ gyttja/soil	mottled to laminated peat/soil/gyttja; inorganic portions primarily silt and clay; commonly < 20 cm thick thickness varies	−10 to −12	transition from upland to coastal; leading edge of transgression
Holocene lagoon	dominantly silt and clay; rare very fine/fine sand; occasional peat; snail (*Urosalpinx cinerea*) shells and shell hash	−11 to surface	backbarrier lagoon; saltmarsh; tidal
Holocene shoreface	heterogenous; dominantly fine to very fine sand; some silt; rare clay; generally coarsening upward; abundant shell (*Mulinia lateralis*) and shell hash	−15 to surface	shoreface; relict shoal
Holocene barrier island and dune	fine to coarse sand; subunits of variable organic content, texture, and grain size include beach, washover, dunes, and interdune swales; swales contain organic-rich silt and wetland species	−7.5 to surface	shoreface, beach, dune, washover, and inlet

Table 4
Seismic stratigraphic units.

Facies Interpretation	Seismic Facies Characteristics	Approximate Depth Range (m)	Corresponding Onshore Stratigraphic Unit Description	Corresponding Unit from Brothers et al. (2020)
Pleistocene shallow marine	low amplitude, low frequency, gently seaward dipping to semi-parallel reflections; appear to downlap poorly resolved lower surface	−20 and deeper	Pleistocene shallow marine shelly mud and sand	Qpp
Pleistocene estuarine	low amplitude, chaotic to semi-parallel and discontinuous reflections; acoustically massive in places; underlying unconformity/base of this unit is high-amplitude, slightly seaward-dipping reflection	−18 to −11	Pleistocene estuarine sands and muds with a base of coarse sand and gravel	upper = Q2 unit; basal = U7 unconformity
Holocene channel/inlet	medium amplitude, low frequency, concave-up reflections	−15 and deeper	not encountered in cores from this study	Qcch
Holocene shoal and sand sheet	medium amplitude, medium frequency parallel sheet-like reflections that generally conform to the seafloor morphology	−5 to - 15	mixed sand and mud Holocene shoreface	Qmn

Tom's Cove Hook (Figs. 6 and 7). The uppermost sections of this unit are resolved in vibracores from central and western Tom's Cove at depths of −5.1 m MSL and deeper.

Radiocarbon dates of shell samples collected from this unit under Fishing Point (modern to 300 cal Yrs. BP, beneath a subaerial beach formed within the last 100 years) indicate recent deposition and likely reworking of the sediment. When paired with sediment texture data and the coarsening-upward trend, this indicates a shoreface depositional environment possibly characterized by migrating sand ridges, such as those found offshore of modern southern Assateague (see Pendleton et al., 2017). The coarsening-upward trend commonly reflects a transition from lower to upper shoreface depositional environments (see Rodriguez et al., 2001; Timmons et al., 2010; Hollis et al., 2019).

This unit extends offshore as the modern Holocene cover of shoals (*i.e.,* shoreface ridges) and sand sheets (Fig. 8, Table 4). In seismic profiles, the unit is marked by medium amplitude, medium frequency, parallel, sheet-like reflections that generally conform to the seafloor morphology and vary from 5 to 15 m in depth and 5–10 m in thickness. It corresponds to the Qmn unit of Brothers et al. (2020), described as a highstand systems tract composed of the modern sandy shoreface. The thickness of this unit increases to the south and east near the southernmost tip of modern Assateague Island (Fig. 8). This spatial variation in thickness is consistent with a Holocene sand thickness map from Wikel (2008) as well as historical bathymetric data which indicate the presence of high-relief shoals offshore of southern Assateague (Fig. 9).

4.2.6. Holocene channel and inlet

This unit contains medium amplitude, low frequency, concave up reflections (Fig. 8; Table 4). While this unit is not encountered in cores from this study, it is consistent in depth (−20 m MSL and deeper) and seismic character with unit Qcch described by Brothers et al. (2020) as channel-fill deposited since the Last Glacial Maximum. As such, it is likely Holocene-age channel and/or inlet fill, possibly (but not definitively) related to the inlet observed by Halsey (1978) underlying Assateague Island near Lighthouse Ridge (see Fig. 5).

4.2.7. Holocene barrier island and dune

The uppermost stratigraphic unit found across all three islands is composed of yellowish brown (Munsell color: 10 YR 5/4) fine to medium sand (median grain size: 0.19–0.52 mm; average sorting: 0.6φ). Radargrams collected from central Chincoteague and Assateague islands show evidence of abundant seaward-dipping (1 − 5° to the southwest) clinoforms in this unit. On Assateague, the presence of chaotic internal GPR reflections differentiate aeolian deposition (*i.e.*, reworking and homogenization of material by aeolian processes) from the underlying beach subunit. However, on Chincoteague, no chaotic internal GPR reflections are observed, as anthropogenic road fill has disturbed aeolian sediments at sites where GPR data were collected (Fig. 4). Data from GPR, shoreline chronology, and sediment cores together indicate that this sandy unit was formed as a series of progradational beach and foredune ridges which comprise the relict (Chincoteague) and modern (Assateague and Wallops) open-ocean barrier islands.

4.3. Sediment volumes and fluxes

Paired analysis of time-varying barrier-island aerial change (OSL dates, shoreline analysis) and barrier thickness (sediment core data) allow for calculation of both fluxes and total volumes of beach and foredune ridge sand captured in this multi-island system, as well as total volumes of the mixed sand and mud shoreface

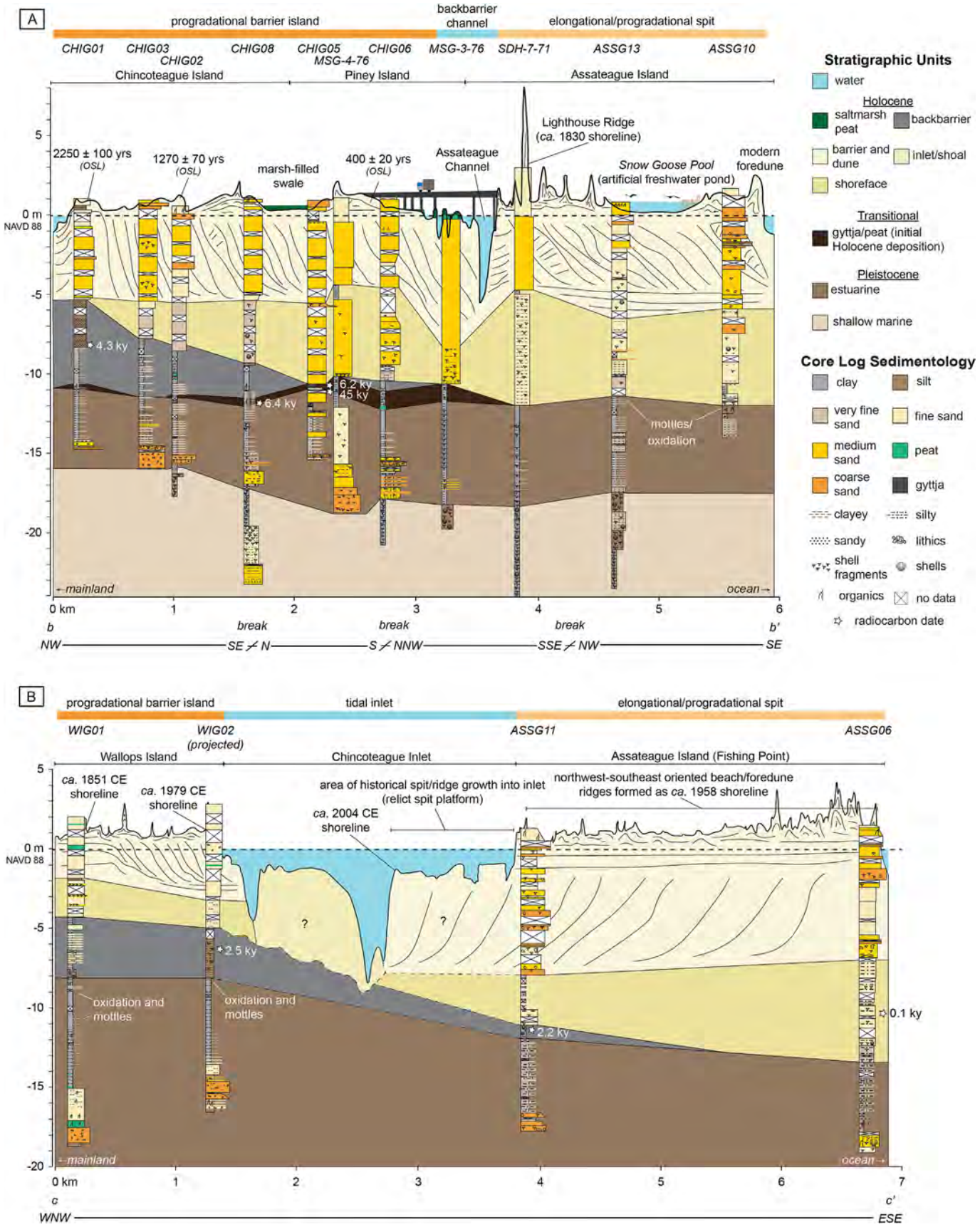

Fig. 6. Detailed stratigraphic cross-sections (top: b-b' and bottom: c-c'; see Fig. 1 for locations) oriented approximately west (mainland) to east (ocean) on A) Chincoteague Island and across Piney Island to the relict recurved spit of Assateague Island. Note multiple changes in orientation given by the "breaks" along the profile; and B) Wallops Island and across Chincoteague Inlet to the modern spit end of Assateague Island. Note: Internal barrier-island bedding is artistically inferred from available ground-penetrating radar profiles.

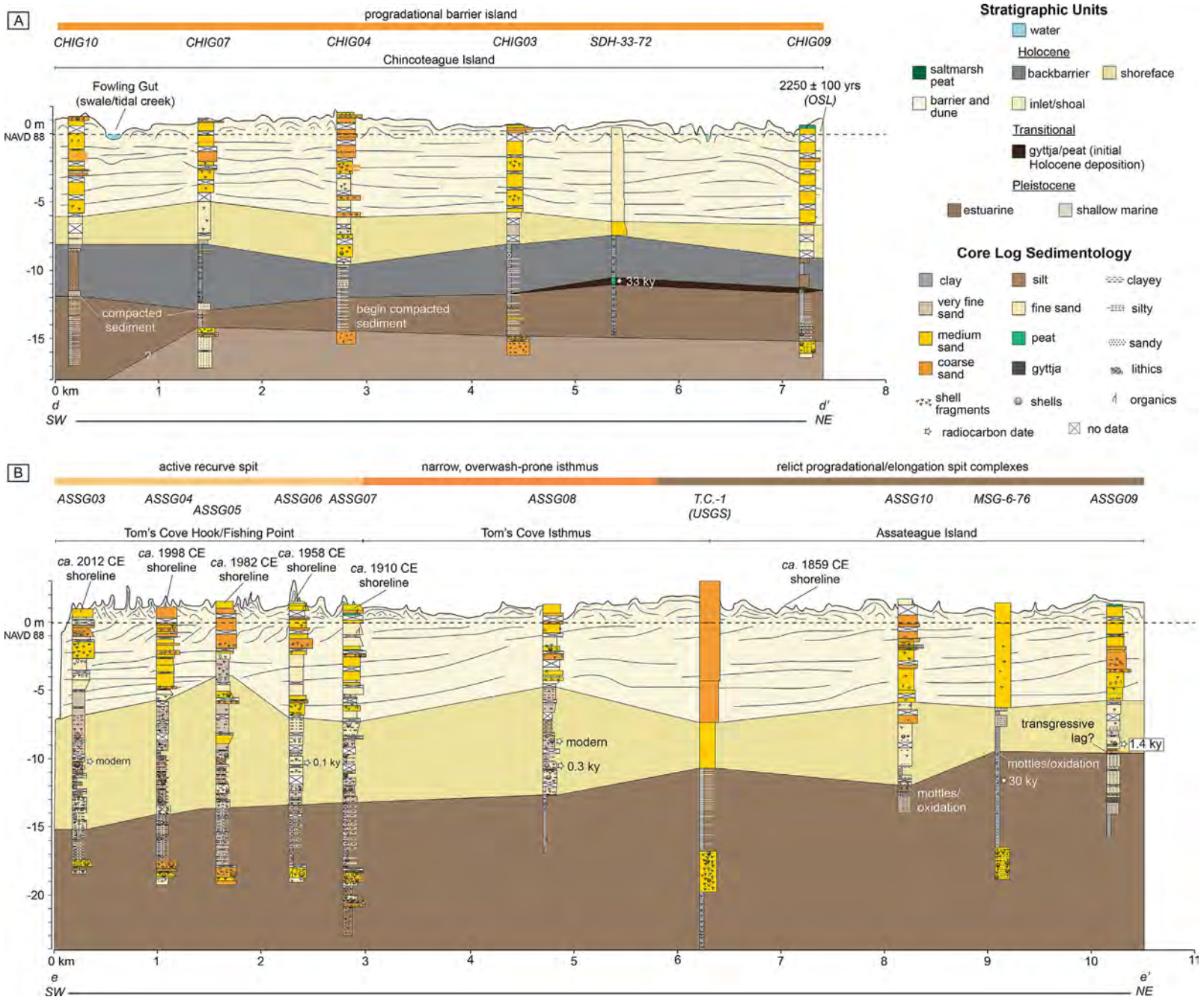

Fig. 7. Detailed stratigraphic cross-sections (top: d-d' and bottom: e-e'; see Fig. 1 for locations) oriented southwest to northeast on A) Chincoteague Island and B) Assateague Island. The Chincoteague Island cross-section is oriented entirely shore-parallel, while the Assateague Island cross-section changes orientation from shore-normal (0–~3.5 km) to shore-parallel (~3.5–10.5 km). Note: Internal barrier-island bedding is artistically inferred from available ground-penetrating radar profiles.

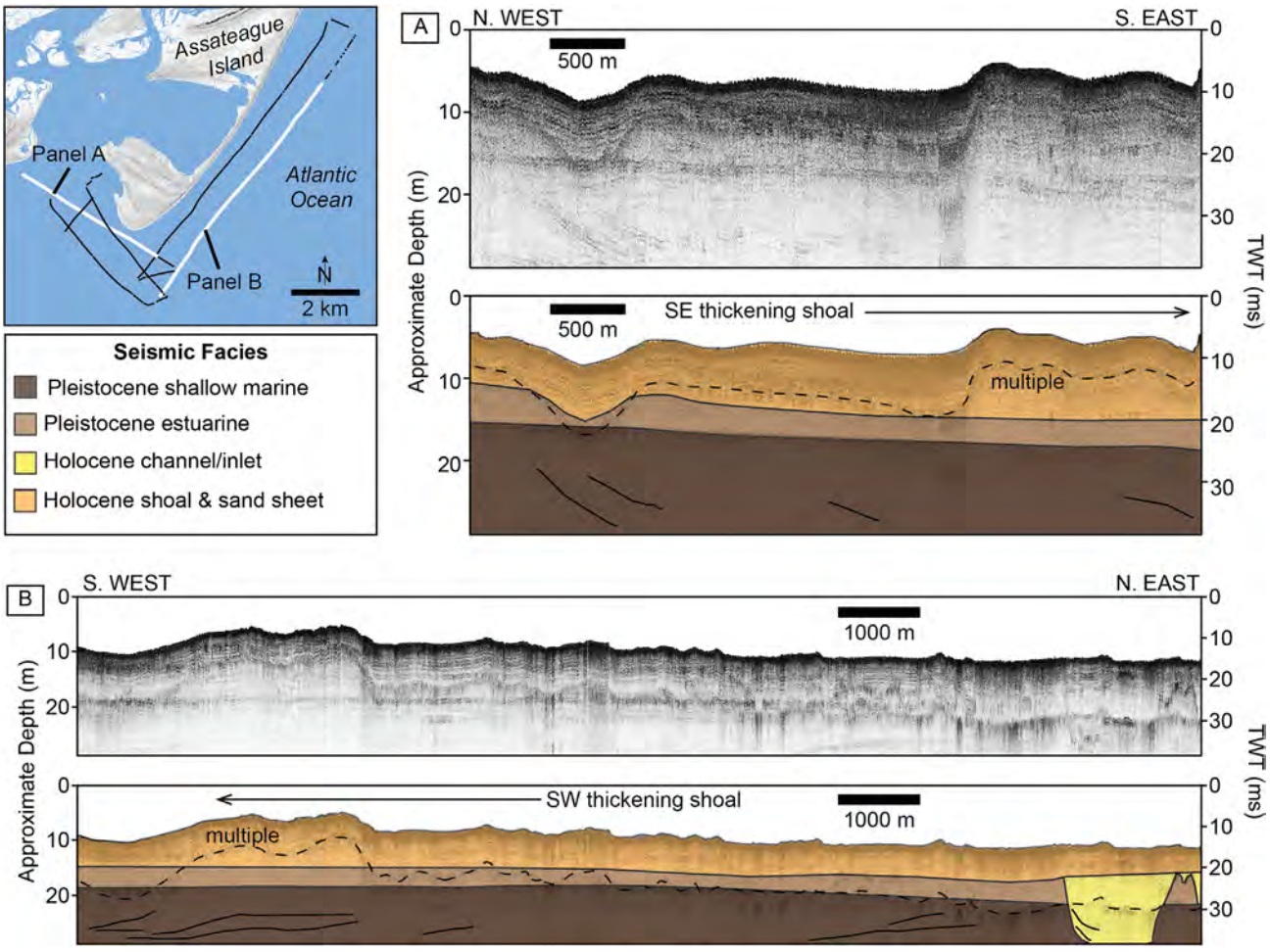

Fig. 8. Seismic stratigraphy of the Assateague-Chincoteague-Wallops barrier-island system. An inset map of seismic lines is included in the upper left corner. A) Processed (top) and interpreted (bottom) northwest-to-southeast (shore-normal) seismic line. Note the thick (~7 m) wedge of Holocene sand. B) Processed (top) and interpreted (bottom) southwest-to-northeast (shore parallel) seismic line that indicates a southwest-ward thickening Holocene shoal and sand sheet unit. In both panels, units (except the channel/inlet fill) correspond to stratigraphic units observed in onshore sediment cores and Brothers et al. (2020) offshore seismic facies.

deposits (Table 5). Chincoteague, Assateague, and Wallops contain 81 million, 127 million, and 7 million m^3 of sand preserved through beach and foredune ridge progradation, respectively. Average sand fluxes trapped during active progradation range from ~40,000 m^3 yr^{-1} (Chincoteague and Wallops) to 681,000 m^3 yr^{-1} (Assateague). On Chincoteague, the relict shoreface unit contains 69 million m^3 of sediment (sand and mud), while Assateague and Wallops preserve 108 million and 4 million m^3 of shoreface sediment, respectively. Over the last *ca.* 120 years, Fishing Point trapped dominantly fine to medium sand with some beds of coarse to very coarse sand (see Supplemental Materials Fig. S1). Progradation of the barrier deposits preserved underlying shoreface deposits which contain dominantly fine sand but also very fine sand, silt, and clay of varying content (see Supplemental Materials Fig. S1).

5. Discussion

5.1. Quaternary deposition at Assateague, Chincoteague, and Wallops islands

We interpret the pre-Holocene and middle Holocene to modern depositional history of the Assateague-Chincoteague-Wallops barrier-island system using an integrated analysis of geochronology, sediment-core data, seismic stratigraphic data, and volume and flux reconstructions (Fig. 10).

5.1.1. Pre-Holocene deposition at Assateague, Chincoteague, and Wallops islands

The Quaternary geologic evolution of the Delmarva Peninsula and proximal continental shelf is marked by a series of sea-level highstands and lowstands which together resulted in a sequence of welded transgressive and regressive coastal barrier, nearshore, estuarine, and fluvial deposits (*e.g.*, Mixon, 1985; Ramsey, 2010; Brothers et al., 2020). The Persimmon Point paleochannel underlies the modern Assateague-Chincoteague-Wallops barrier system and likely formed during Marine Isotope Stage 22 (~866 ka), 16 (~676 ka), or 12 (~478 ka) by the flow of the Susquehanna and Potomac rivers (Brothers et al., 2020). While data from this study do not resolve this subaerial unconformity, our seismic data and cores do indicate that infilling of this paleochannel occurred during the Pleistocene, likely in the form of a transgressive systems tract (Brothers et al., 2020) composed of primarily marine and estuarine deposits. A Pleistocene-age transgressive ravinement surface overlies this feature (U7 per Brothers et al., 2020) and the base of the overlying unit contains coarse, reworked sediment, possibly of fluvial origin. The youngest Pleistocene deposits underlying the

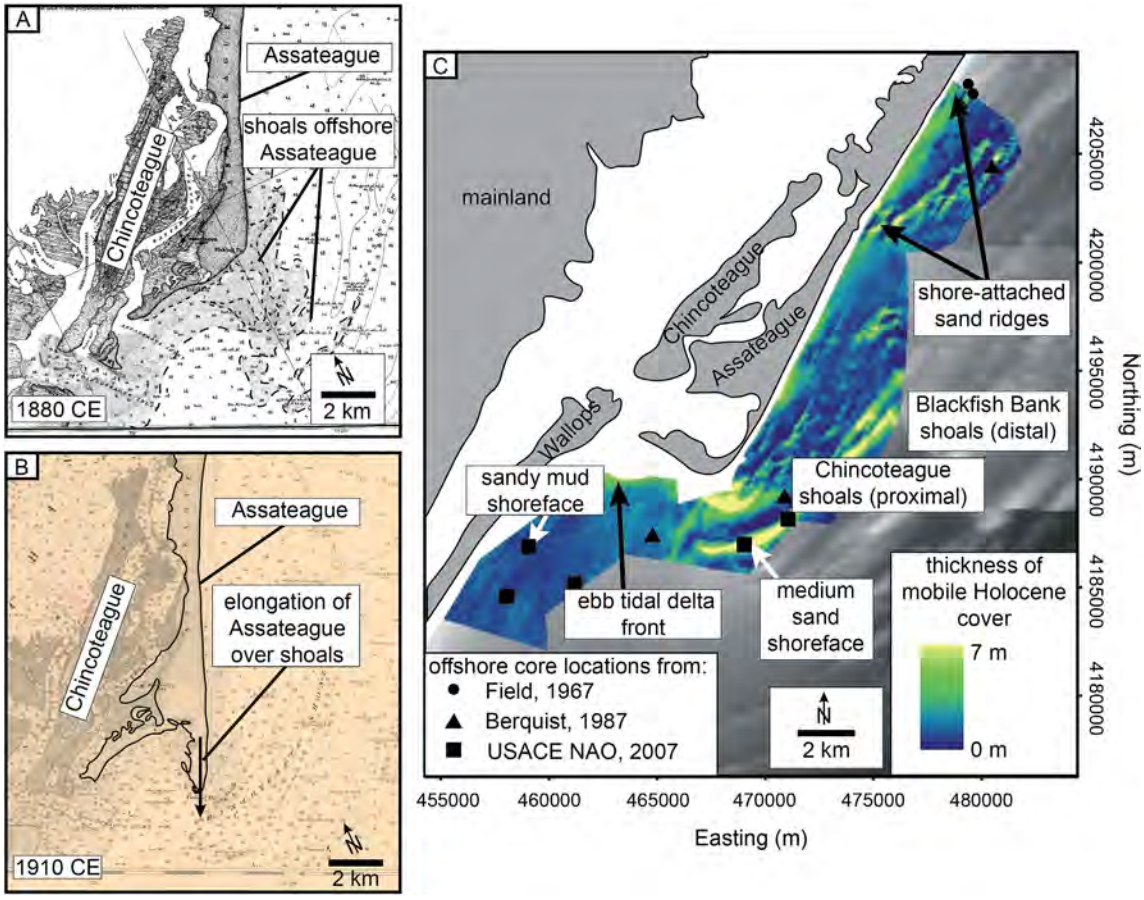

Fig. 9. Historical development of southern Assateague Island and proximal nearshore bathymetric features. A) Southern Assateague Island and shoreface in 1880 CE. Note the subaqueous offshore shoals. Modified from a map published by U.S. Coast Survey (1880). B) By 1910 CE Assateague Island had migrated directly over the shallow platform provided by the subaqueous shoals. Modified from a map published by the U.S. Coast and Geodetic Survey (1910) C) Offshore shoals are located proximal to the contemporary (*ca.* 2008) spit, likely acting as a control on offshore accommodation. Note: Map modified from Wikel (2008) using data collected in 2004/2005. Shoreline positions shown are *ca.* 1980s. White arrows and associated sediment descriptions reference sediment cores analyzed by Wikel (2008).

Table 5
Field site volumes and fluxes.

Depositional Environment	Time 1	Time 2	Duration (years)	Area (millions m^2)	Thickness (m)[a]	Volume (millions m^3)[b]	Flux (thousands m^3 yr^{-1})
Chincoteague Barrier Phase 1	2250 ± 100	1270 ± 70	980	7.2	5.8	44	44
Chincoteague Barrier Phase 2	1270 ± 70	400 ± 20	870	6.5	5.9	40	46
Chincoteague Barrier Total	**2250 ± 100**	**400 ± 20**	**1850**	**13.8**	**5.8**	**81**	**44**
Assateague Spit Phase 1	1830 CE	1910 CE	80	12.9	6.5	87	1082
Assateague Spit Phase 2	1910 CE	2017 CE	107	5.1	7.7	43	405
Assateague Spit Total	**1830 CE**	**2017 CE**	**187**	**18.1**	**6.8**	**127**	**681**
Wallops Barrier Total	**1851 CE**	**2017 CE**	**166**	**1.7**	**4.2**	**7**	**42**
Chincoteague Shoreface Total	–	–	–	13.8	5.0	69	–
Assateague Shoreface Total	–	–	–	18.1	6.0	108	–
Wallops Shoreface Total	–	–	–	1.7	2.5	4	–

[a] Thickness estimates from sediment cores and lidar topography (USGS, 2016).
[b] Includes foreshore volume estimate for final year of calculation. See Methods for detail.

Assateague-Chincoteague-Wallops barrier system consist of estuarine sediments and represent a highstand systems tract.

5.1.2. Stage I – Migration of Chincoteague/Wallops: Wave erosion of backbarrier deposits

Starting 6000 years ago, initial backbarrier deposition occurred in the proto-Wallops and Chincoteague backbarriers (Fig. 10a), consistent with data from other barrier-backbarrier systems across the Maryland and Virginia coasts (*e.g.*, Finkelstein and Ferland, 1987; Raff et al., 2018; Shawler et al., 2021). Preservation of backbarrier deposits is coincident with an apparent deceleration in relative sea-level rise from ~2 to ~1.5 mm yr^{-1} (Engelhart and Horton, 2012; Raff et al., 2018). If barriers existed earlier, they likely were situated much farther offshore, and the shelf would contain the only preserved deposits associated with proto- and incipient barriers (Swift, 1975; Finkelstein and Ferland, 1987).

Transgression dominated the net behavior of the barrier system from *ca.* 6000 to 2250 years ago. Tidal inlet and overwash processes led to net barrier rollover. While periods of barrier stabilization or even progradation may have occurred, they are not recorded in

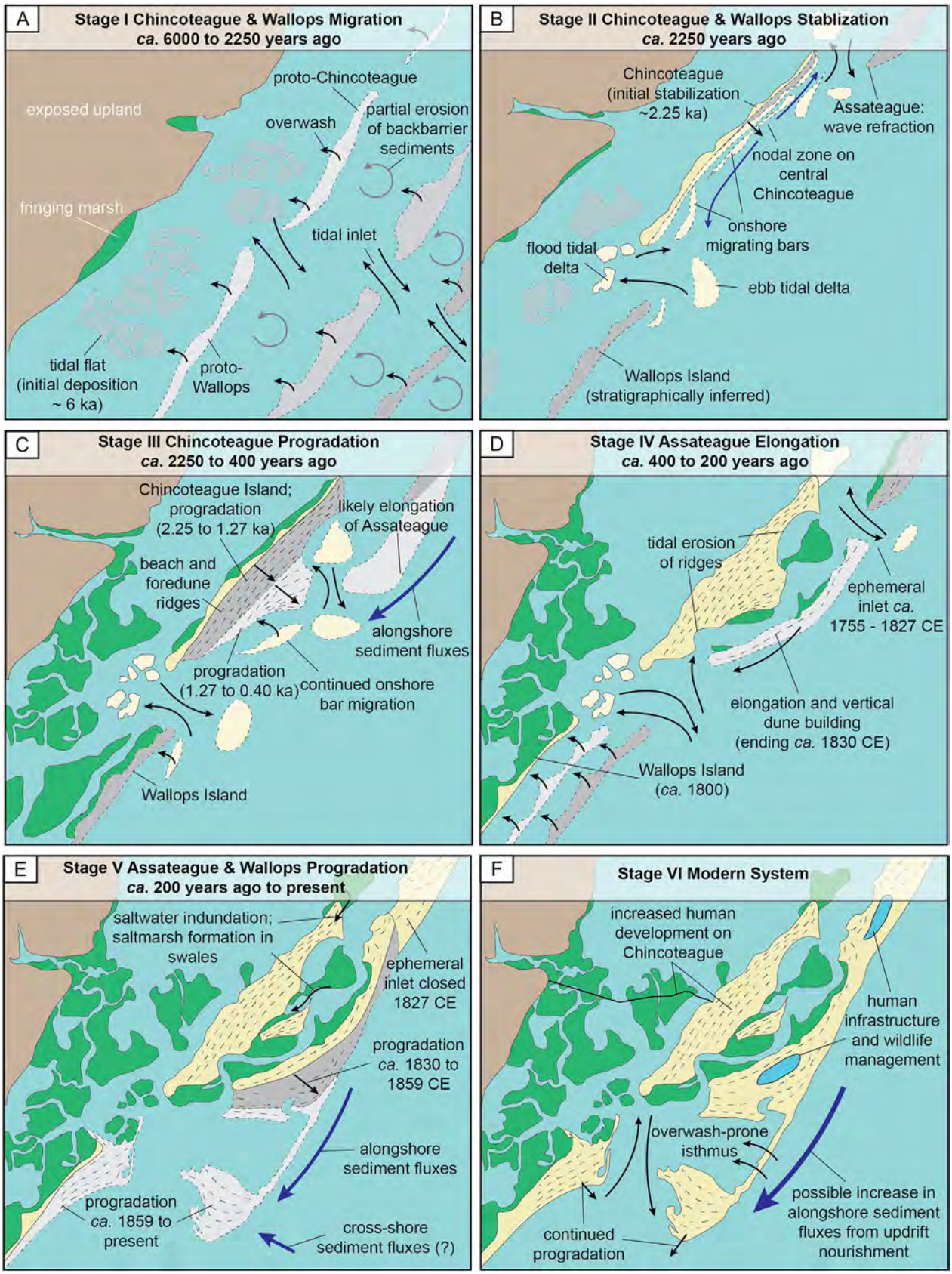

Fig. 10. Planform evolutionary model of the development of the Assateague-Chincoteague-Wallops barrier complex. In all panels, the darkest gray features are oldest, and the lightest gray features are youngest. A) Stage I: Prior to ~2.25 ka, net landward migration of the barrier system occurred in a regime of slow relative sea-level rise (~1 mm yr^{-1}); B) Stage II: Around 2.25 ka Wallops was located offshore of its present location, and the initial progradation of Chincoteague was driven by high alongshore and onshore sediment fluxes, primarily via onshore migration of bars. A nodal zone of diverging longshore transport directions developed on Chincoteague, controlled by wave refraction around the

these data. As the barriers migrated landward, waves and currents eroded backbarrier sediments exposed on the shoreface, leading to preservation of relict backbarrier deposits which pinch out in a seaward direction. Given the net landward migration of the barrier systems, only these backbarrier deposits are preserved.

5.1.3. Stage II – Stabilization of Chincoteague Island: Sediment supply as a control on barrier state changes

About 2250 years ago, Chincoteague Island stabilized at or near the location of its western-most ridge and Wallops Island was offshore of its present location (Fig. 10b). Myriad factors likely contributed to the timing and location of the stabilization of Chincoteague Island. Complex antecedent morphology, as explored in depth as a factor in barrier-island migration by Shawler et al. (2021), is an unlikely control here, as the antecedent surface underlying Chincoteague and Wallops islands is largely planar and lacks the elevated surfaces upon which barrier islands to the south were pinned. However, shoreface sediment fluxes may have played an important role. For example, many of Virginia's barrier islands are particularly sensitive to subtle changes in sediment delivery rates, which may control state changes between landward migration and stabilization/progradation (Ciarletta et al., 2019b, 2021). A range of factors can control variations in cross-shore and longshore sand fluxes along this coast, including ebb-tidal delta configuration (Fenster et al., 2016), inlet sediment bypassing (Fenster and Dolan, 1996), backbarrier sand trapping (Seminack and McBride, 2015b, 2019), excavation of antecedent sediment (Raff et al., 2018; Shawler et al., 2021) by ephemeral tidal inlets, and modified wave refraction patterns and sediment trapping associated with the growth of updrift spits and ebb-tidal deltas (Fenster et al., 2016; Jones, 2016). An unknown combination of such processes likely temporarily increased sediment fluxes to Chincoteague Island around 2250 years ago and led to the associated transition from retrogradation to progradation of the island. Additionally, this period of island stabilization corresponds to a decrease in storminess and likely associated reduction in overwash fluxes and island dissection/breaching, as observed at other U.S. East Coast barrier sites (*e.g.*, Mallinson et al., 2011).

5.1.4. Stage III – Progradation of Chincoteague Island: Formation of a large Holocene sand deposit

Initial progradation of Chincoteague Island began *ca.* 2250 years ago and lasted until *ca.* 400 years ago (Fig. 10c). While the net dip directions of reflections in shore-normal radargrams along Chincoteague Island are seaward, there is also evidence of shallow, landward-dipping reflections (see Fig. 4), indicative of progradation through onshore migration and welding of swash bars (*e.g.*, Hine, 1979; Carter, 1986; Nooren et al., 2017). We suggest that progradation of Chincoteague Island was driven by ebb-delta-associated sediment bypassing at tidal inlets immediately north and south of the island, as observed along inlet-adjacent shorelines throughout the Virginia Barrier Islands (*e.g.*, (Fenster and Dolan, 1996). To the north of Chincoteague Island, wave refraction around what was then the southern terminus of Assateague Island and an ebb-tidal delta associated with the southeast-northwest-oriented inlet separating Chincoteague and Assateague islands likely created a nodal zone (region of divergent longshore transport) on central Chincoteague. Sediment was directed away from this region, both to the north and south along the Chincoteague shoreline. To the north, this sediment entered the semi-protected coastal reach landward of southern-most Assateague Island, and accumulated in a wave-shadow zone in the form of beach and foredune ridges. In this manner, Chincoteague Island underwent a period of widening similar to that observed for modern Wallops Island, where a nodal zone—located along the central part of the island and caused by wave refraction around southern Assateague—leads to diverging sediment fluxes, net northerly transport along the northern end of the island, and the eastward growth of beach and foredune ridges along the northern depocenter (Fenster and Bundick, 2015).

The growing shoreface and beach and foredune ridges of Chincoteague Island incorporated approximately 81 million m^3 of sand which otherwise likely would have been transported to downdrift barriers. However, the annual sand trapping flux varied with time. From *ca.* 2250 to 1300 years ago the barrier volume grew by an average of ~44,000 $m^3\ yr^{-1}$ and ~46,000 $m^3\ yr^{-1}$ between *ca.* 1300 to 400 years ago (Table 5; Fig. 11). This suggests that sediment retention rates within Chincoteague Island did not substantially change with time and the impact of Chincoteague's widening on downdrift sand fluxes likely remained constant. However, the sand supply to individual downdrift barriers was also dependent on other local processes, such as changes in ebb-tidal delta sediment bypassing, cross-shore sediment fluxes, and tidal and wave ravinement of antecedent geology (*e.g.*, Fenster et al., 2016; Raff et al., 2018; Shawler et al., 2019b; Shawler et al., 2021).

5.1.5. Stage IV – Elongation of Assateague Island: Importance of updrift inlets and barrier connectivity

A period of little to no deposition occurred in the Assateague-Chincoteague-Wallops system when tidal inlets became more prominent updrift on Assateague (Fig. 11). Between *ca.* 1620 CE and 1755 CE, Assateague Island elongated 4 km to the south and seaward of Chincoteague, forming an initial recurved spit. The opening of five ephemeral inlets along northern and central Assateague (~3–~28 km north of Lighthouse Ridge) between *ca.* 1755 CE and 1830 CE (Seminack and McBride, 2015) temporarily stopped the elongation/progradation of Assateague Island. We estimate the volumes of sand trapped in the flood tidal deltas of Cherry Tree (~3 km updrift) and Green Run (~14 km updrift) inlets using aerial mapping of inlet-associated features identified by Seminack and McBride (2015), paired with average regional flood tidal delta thickness values (~3 m thick) from Seminack and McBride (2019). The estimates indicate that the fluxes of sediment into growing flood-tidal deltas of these two inlets possibly reduced longshore transport to the Assateague-Chincoteague-Wallops system by as much as ~222,000 $m^3\ yr^{-1}$ (20% of post-1830 CE fluxes; >100% of pre-1830 CE fluxes) during the period of active inlet activity. This resulted in limited downdrift progradation between *ca.* 400 and 190 years ago (Fig. 10d). We hypothesize that continued fluxes of fine sand from the beach and nearshore system to the adjacent dunes during this period allowed for aggradation of the 8+ m tall aeolian ridge (Lighthouse Ridge). Conceptual (Psuty, 2004) and morphodynamic (Ciarletta et al., 2019b) models link similar periods of dune-building with slowed shoreline progradation, an observation confirmed by local (*e.g.*, Parramore Island, Virginia; Raff et al., 2018), regional (*e.g.*,Cape Lookout, North Carolina; Elliott et al.,

southern terminus of Assateague Island; C) Stage III: Progradation of Chincoteague continued through progressive welding off bars by inlet sediment bypassing and subsequent reworking of sand by longshore transport processes; the southward elongation of Assateague is inferred from the shifting nodal zone evident in the ridge orientation on Chincoteague; D) Stage IV: Assateague Island began to elongate seaward of Chincoteague Island. The exact timing of this multi-stage development is unknown, but it likely occurred between *ca.* 1620 CE and 1755 CE. The immediately updrift Cherry Tree Inlet was ephemerally open between 1755 CE and 1827 CE, thereby halting or greatly slowing downdrift progradation and, instead, allowing for vertical dune building of Lighthouse Ridge (8+ m tall).; E) Stage V: The progradation (net direction NW to SE) of southern Assateague was driven by cross-shore sediment fluxes combined with increased alongshore sand fluxes from closure of updrift inlets, which previously functioned as a sediment trap. F) Stage VI: The modern system continues to elongate/prograde and is marked by increased human infrastructure.

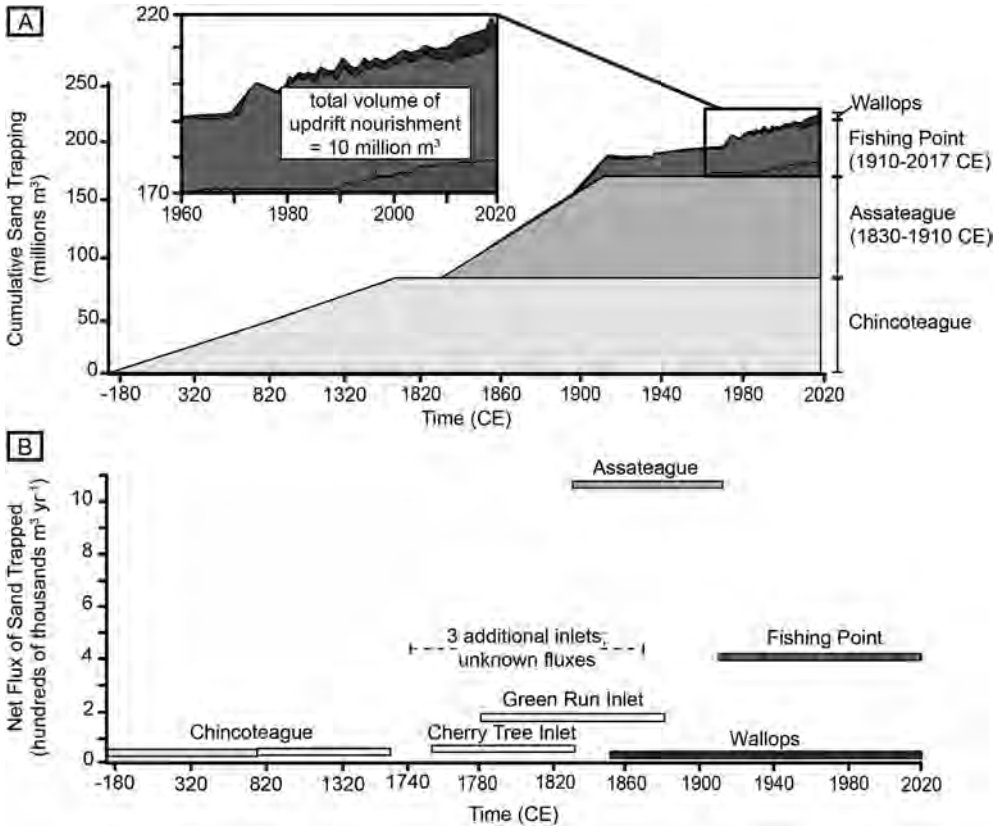

Fig. 11. Volumes and fluxes of sand through time for the Assateague-Chincoteague-Wallops barrier system. A) Cumulative sand trapping over the last *ca.* 2250 years showing the relative contribution of each depositional feature. Updrift nourishment refers to sediment placed on beaches from Ocean City, MD (~60 km updrift) and northern Assateague Island (~55 km updrift) (source: The National Beach Nourishment Database [Campbell and Benedet, 2006; ASBPA, 2020; Elko et al., 2021]). The data indicate that natural sediment trapping through barrier-island progradation and spit elongation overwhelms any major contribution from alongshore transport of artificially placed updrift sediment. Note the change in horizontal scale starting at 1820 CE. B) Time-varying average fluxes of sand trapped in each depositional feature through time. A period of no/little deposition in the Assateague-Chincoteague-Wallops system corresponds to a period of heightened updrift inlet activity from 1740 to 1830 CE. Estimates of fluxes into two of those inlets are calculated from aerial mapping of flood tidal delta area, supplemented by representative sediment core data from Seminack and McBride (2019). Note the change in horizontal axis scale starting at 1740 CE.

2015), and global (*e.g.*, Pedro Beach, Australia; Oliver et al., 2019b) field studies.

5.1.6. Stage V – Progradation/elongation of Assateague and Wallops islands: Shoals as a framework control on spit development

Southerly elongation of Assateague Island resumed in *ca.* 1830 CE and lasted to 1910 CE, during which time the barrier trapped ~87 million m^3 of sand through the accelerated formation of a beach- and foredune-ridge plain and the development of a narrow isthmus. Fluxes to the system were around 1 million m^3 per year during this phase (Fig. 11). The onset of this period of rapid progradation coincided with the closure of both the proximal Cherry Tree Inlet and the more distal ephemeral Sinepuxent Inlet (~24 km north of Lighthouse Ridge). Alongshore fluxes were likely further enhanced by the closure of North Beach (~28 km north) and Green Run (~14 km north) inlets in 1840 CE and 1880 CE, respectively (Goettle, 1978; Seminack and McBride, 2015). With the closure of both inlets, sand delivery to backbarrier flood-tidal deltas ceased and ebb-tidal deltas collapsed, together increasing downdrift sand fluxes to southern Assateague Island. Furthermore, the growth of Assateague during this time coincides with state shifts of islands south (downdrift) of Assateague, including landward migration and rapid thinning (by over 200 m) of Metompkin Island (Byrnes, 1988; Deaton et al., 2017), accelerated migration of Cedar Island (starting *ca.* 1852 CE; Shawler et al., 2019b), and rapid erosion of southern Parramore Island (starting *ca.* 1870 CE; Raff et al., 2018). Taken together, these observations indicate the possible importance of sand fluxes between updrift inlets and downdrift spits, and, by extension, interconnections between elongating spits and the behavior of downdrift barrier islands.

In the late 1800s, Assateague Island continued to elongate in a southwesterly to southerly direction (Fig. 10e). An isthmus formed south of the 1859 CE shoreline and by 1910 CE extended over a series of shoals/shoreface ridges (Fig. 9b). We propose that the offshore and shoreface-attached shoals south of Assateague Island acted as a framework control on accommodation by providing a platform upon which the spit could rapidly prograde, eventually determining the subaerial morphology of the Tom's Cove Isthmus. Stratigraphic data from this study indicate that the isthmus, as well as the entire recurved spit (formed from 1910 CE to present), is underlain by shoreface sediment of a consistent depth (−5 to −6 m MSL). The growth of the isthmus and recurved spit created the shallow Tom's Cove in which fine sediments could settle in the quiet-water embayment atop the underlying shoreface sediment. The shoals provided comparatively uniform, shallow accommodation which differs from the deeper (below −10 m MSL) adjacent shoreface. Recent shoreface mapping (Wikel, 2008, Fig. 9c) and seismic stratigraphy from this study (Fig. 8) indicate the presence of thick (up to 7 m) shoals offshore of modern Assateague that may provide a shallow platform for continued/future spit progradation.

Since 1851 CE, the northernmost portion of Wallops Island has prograded to the north and east. During this time, northern

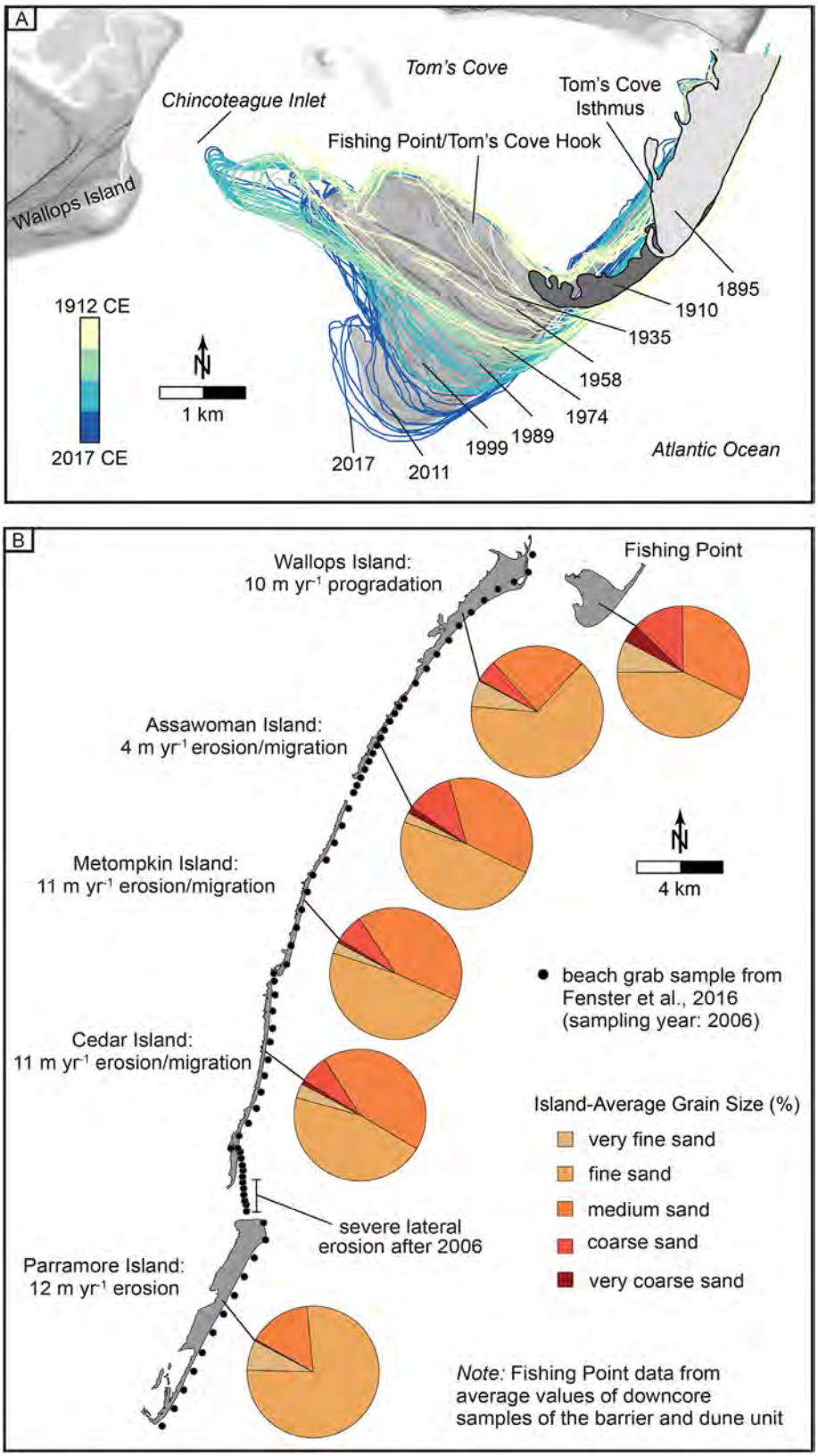

Fig. 12. Evidence of historical sediment trapping. A) Fishing Point shoreline change. Modified from Hein et al. (2019b). B) Average grain-size distribution of sediment within the barrier and dune unit sampled in sediment cores across Fishing Point (representative of beach sediments deposited between 1920 and 2015 CE) and shallow (5–20 cm deep) samples from 1 m above the high-water line on downdrift barrier-island beaches. Data from Fishing Point are from this study, while beach grain-size data are from Fenster et al. (2016). Island-average shoreline retreat rates are from Deaton et al. (2017) for the period 1980–2010 CE.

Wallops trapped 7 million m^3 of sand at an average rate of 42,000 m^3 yr^{-1} (Table 5; Fig. 11). An additional 4 million m^3 of mixed sand and mud was preserved as the barrier grew over the shoreface. Since 1910 CE, the elongation of southernmost Assateague Island has trapped 43 million m^3 of sand at a rate of over 400,000 m^3 yr^{-1} (Table 5; Fig. 11). During this time, the downdrift Metompkin, Cedar, and Parramore islands have rapidly eroded and/or migrated landward at long-term (1850–2010 CE) average rates of $\geq$4 m yr^{-1} and short-term (1980–2010 CE) average rates of $\geq$10 m yr^{-1} (Deaton et al., 2017). Today, both southern Assateague and northern Wallops islands function as sediment sinks through continued growth of beach and foredune ridges.

5.1.7. Stage VI – Modern system: human intervention in the sediment transport system

Modern coastal change along the Assateague-Chincoteague-Wallops barrier-island complex occurs in response to both natural and human influences. The recurved spit at the terminus of Assateague Island continues to grow southward, and northernmost Wallops Island continues to widen to the east and elongate to the north. By contrast, the narrow isthmus on southern Assateague occasionally breaches and is now located ~700 m landward of its late 19th and early 20th century position. This landward migration is likely to continue as the isthmus is frequently overwashed and/or breached by storms, which leads to sand deposition in the barrier-proximal (*i.e.*, eastern) portion of Tom's Cove. Progradation of the entire system has occurred since *ca.* 2250 years ago through the natural influx of sand through longshore transport. However, since *ca.* 1961, the system has likely received additional inputs supplied from the reworking of updrift beach nourishment sands (Fig. 11). Yet, this artificial, short-term nourishment flux—even in the highly unlikely case that 100% of it were transferred to downdrift reservoirs—pales in comparison to natural (*i.e.*, pre-nourishment) sand trapping in this system; over the last 60 years, updrift nourishment volumes along the beaches of Ocean City, Maryland (~60 km north) and northern Assateague Island (~55 km north) combine for only ~10 million m^3 of sand, as compared with the ~30 million m^3 of sand captured by Fishing Point/Wallops Island over this same time.

On Wallops Island, recent anthropogenic modifications include beach nourishment (since 2010; 3 million m^3 of sand in total) and ongoing efforts to stabilize a seawall that has existed since 1945 CE (Fenster and Bundick, 2015). Additionally, the youngest beach/foredune ridge on northern Wallops is being mined as a source of nourishment sand for an ongoing (as of July 2021 CE) central Wallops Island breakwater project (NASA, 2019). Predictions of future trajectories for this portion of the system must account for both the natural changes and human dynamics, such as anthropogenic shoreline-control and sediment-management efforts (see Miselis and Lorenzo-Trueba, 2017; Armstrong and Lazarus, 2019; Lazarus and Goldstein, 2019).

5.2. Implications for regional sediment transport

5.2.1. Sand trapping at southern Assateague Island

Net shoreline erosion along the Virginia Barrier Islands downdrift of Wallops Island has increased from a system-wide long-term rate of 5 m yr^{-1} (1870–2010 CE) to 7 m yr^{-1} in the period between 1980 CE and 2010 CE (Deaton et al., 2017, Fig. 12a). Assawoman, Metompkin, and Cedar islands have experienced rapid short-term historical shoreline transgression (4–11 m yr^{-1} on average between 1980 and 2010 CE) largely resulting from landward island migration, and resulting in a geomorphic feature termed the 'arc of erosion', which extends over 35 km south of southernmost Assateague Island (*e.g.*, Rice and Leatherman, 1983; Kraus and Galgano, 2001; Nebel et al., 2012; Fenster et al., 2016; Deaton et al., 2017). South of Cedar Island, Parramore Island is undergoing accelerating erosion, and may enter this same low-relief, washover-dominated regime in the coming decades (Raff et al., 2018).

Four mechanisms may individually or (more likely) collectively explain this observed acceleration and southerly extension in island erosion and landward migration over the historical period: 1) increased storm frequency (*e.g.*, Hayden and Hayden, 2003; Komar and Allan, 2008; 2) increased rates of sea-level rise along the Virginia coast and attendant tidal prism changes (Fenster et al., 2011; Deaton et al., 2017; FitzGerald et al., 2018); 3) changes to the alongshore transport gradient from north to south caused by changing wave refraction patterns around the southern end of Assateague Island (Jones, 2016); and 4) sediment trapping at the recurved spit of southern Assateague (Fenster et al., 2016).

Here, we quantify sediment volumes at southern Assateague Island to constrain the role of growth of these updrift siliciclastic landforms in modifying downdrift barrier behavior. Since the 19th century, Assateague and Wallops islands have together trapped 134 million m^3 of sand at a rate of 720,000 m^3 yr^{-1}. Yet, these trapping magnitudes are unequal: the average flux of sand trapped at Assateague is ten times greater than that trapped at Wallops Island. The grain-size distributions of this sand are roughly equivalent to those found along the beaches of Assawoman, Metompkin, Cedar, and Parramore islands (Fenster et al., 2016). This finding suggests that the sediment trapped on southern Assateague Island consists of an appropriate texture to contribute to the downdrift barrier beaches (Fig. 12b). Additionally, the subaqueous shoals and/or shoreface deposits over which Assateague and Wallops islands prograded represent an additional sediment reservoir of 113 million m^3. However, much of this material consists of heterogeneous sand and mud and therefore is too fine to function as "beach quality" sand for downdrift barrier islands. While we account for sediment trapping through barrier-island progradation and the attendant burial of shoreface sediment, sediment transport and/or trapping mechanisms on the modern shoreface of southern Assateague is/are poorly understood. Landward and downdrift movement of offshore sand ridges is evident and possibly linked with shoreline behavior on Assateague Island (Wikel, 2008; Pendleton et al., 2017). However, the exact sediment transport pathways, mechanisms, and timescales remain unclear. Future work must account the influence of shoreface sand ridges and other framework geologic features on hydrodynamic and sediment transport/storage processes.

A compilation of seven engineering reports and studies conducted between 1956 and 2005 demonstrates that longshore transport along the Assateague Island coast ranges from 115,000 to 1,100,000 m^3 yr^{-1}, with all but one value clustering between 115,000 and 460,000 m^3 yr^{-1} (Fenster and McBride, 2015). The one outlier (1,100,000 m^3 yr^{-1}) is based on wave refraction using wave gauge data from ~125 km south of Lighthouse Ridge (Headland et al., 1987). Based on these estimates, we conclude that Assateague and Wallops islands annually trap a sand volume equivalent to at least 60% of that transported along the Virginia coast north of Assateague Island; removing the Headland et al. (1987) value, trapping fluxes exceed longshore transport rates by as much as a factor of six. This suggests that true transport fluxes are closer to the upper-end estimate ($\geq$1 million m^3 yr^{-1}) and/or that significant volumes of sediment are contributed from the inner shelf. Further complicating this, the flood- and ebb-tidal delta complexes at Chincoteague Inlet represent an additional, but unquantified, sediment/sand sink.

From this analysis, it is clear that growth of the Assateague-Chincoteague-Wallops barrier-island complex represents a very significant longshore sediment sink along the northern Virginia coast. Furthermore, we propose that, in addition to changing

patterns of wave refraction and associated alongshore north-to-south transport gradients (*e.g.*, Jones, 2016), this process is predominantly responsible for net erosional conditions experienced from Assawoman to Parramore islands. The downdrift erosion observed along the most vulnerable reaches is amplified by a sand-poor shoreface and sediment sequestration within large ebb-tidal deltas south of Assateague (*e.g.*, Fenster et al., 2011; Fenster et al., 2016). These results are consistent with observations along the Alabama-Mississippi coast, which indicate the important role that sediment deficits, in addition to storms and sea-level rise, play in barrier island land loss (Morton, 2008; Eisemann et al., 2018; Hollis et al., 2019; Gal et al., 2021). Similar alongshore couplings exist along the Danish Wadden Sea coast, where an alongshore transport gradient from updrift (sediment loss) to downdrift (high sediment supply) results in progradation of the downdrift coast (Fruergaard et al., 2019).

In contrast to sand trapping and alongshore wave gradients, factors which are often recognized as responsible for barrier-island change (*e.g.*, storms, sea-level rise) are likely to affect the Virginia Barrier Islands uniformly. These therefore cannot explain the longshore gradients in barrier behavior. While differential responses to storm events can lead to intra-island variations in barrier morphology (*e.g.*, Houser et al., 2008), a single storm will typically affect a large region (*i.e.*, the full Virginia Barrier Island chain), eroding barrier islands and moving sand alongshore, temporarily offshore, or permanently landward via overwash. Likewise, relative sea-level rise is similar across the southern Delmarva Peninsula, and will therefore impact all barriers in the chain in a similar manner; in this case, by creating additional accommodation and forcing complex barrier behavior including continued retreat (Moore et al., 2010; Lorenzo-Trueba and Ashton, 2014). Beyond the "arc of erosion", additional local factors which

Table 6
Global examples of large longshore sediment traps.

Location	Landform Type	Estimated Total Volume (millions m^3)	Estimated Average Flux During Formation (thousands m^3/yr)	Long-Term Progradation Rate (m/yr)	Data Source(s)	Note
Assateague Island, Virginia, USA	Spit	127	681	25–40	**this study**	since 1830 only
Matagorda Island, Texas, USA	Progradational Barrier Island	2300	275	*~0.4*	Wilkinson (1975)	
Fire Island, New York. USA	Spit	–	165	–	Hoan et al. (2011)	modeled value
Pinheira Strandplain, Brazil	Strandplain	910	*157*	1–2	Hein et al. (2013); Hein et al. (2015)	
Navegantes Strandplain, Brazil	Strandplain	580	*100*	1	FtizGerald et al. (2007); Hein et al. (2014b); Hein et al. (2015)	
King Point, Yukon Territory, Canada	Spit	9	*100*	–	Hill (1990)	mixed sand and gravel; volume in 1985
Kaitorete "Spit", Canterbury, New Zealand	Barrier	700	*88*	1–13	Soons et al. (1997)	longshore-fed supply of gravel; volume in 1994
Chincoteague Island, Virginia, USA	Progradational Barrier Island	81	44	1–1.8	**this study**	
Vejers Spit, Denmark	Spit	*175*	*44*	1	Nielsen et al. (1995)	
Guichen Bay, Australia	Strandplain	*318*	44	0.43–7.8	Oliver et al. (2019a) and Bristow and Pucillo (2006)	
Wallops Island, Virginia, USA	Progradational Barrier Island	7	42	0.8–10	**this study**	northern island only
Rivoli Bay, Australia	Beach Ridge Plain	*237*	34	0.38	Oliver et al. (2019a)	
Jurerê Strandplain, Brazil	Strandplain	110	25	0.82	Hein et al. (2019b)	
Miquelon-Langlade Barrier, Gulf of St. Lawrence	Composite Barrier	65	*22*	0.3–0.75	Billy et al. (2018)	mixed sand and gravel
Bug Peninsula, NW Rügen, Germany	Spit	66	*17*	–	Naumann et al. (2009)	
Pedro Beach, Australia	Strandplain	43	14	0.38–1.2	Oliver et al. (2019b); Oliver et al., (2020)	
Daniela Spit, Brazil	Spit	4	4	3	Hein et al. (2019b)	
Sillon de Talbert Spit, Brittany, France	Spit (migrational)	1	3	–	Stephan et al. (2012)	gravel barrier; sediment recycling (no major source)
Lubec Spit, Maine, USA	Spit	*0.1*	1	0.4–3	Kelley et al. (2015)	mixed sand and gravel; volume in 2012
Wells-Ogunquit Barrier Complex, Maine, USA	Multi-Barrier Complex	32	–	–	Van Heteren et al. (1996); Montello et al. (1992)	multiple mainland segmented bariers/spits
Saco Bay barrier, Maine, USA	Multi-Barrier Complex	22	–	–	Van Heteren et al. (1996)	multiple mainland segmented bariers/spits
Mignuk Spit, Canada	Spit (erosional)	0.3	–	–	Hequette and Ruz (1991)	mixed sand and gravel; volume in 1985
Popponesset Spit, Masschusetts, USA	Spit (erosional/ ephemeral)	0.3	–	–	Aubery and Gaines (1982)	volume in 1954

Note: *Italicized* values were calculated using data available in the reference(s); landforms sorted by average flux.

may control differential future behavior of individual islands include variable underlying stratigraphy (*e.g.,* Brenner et al., 2015), complex antecedent morphology (*e.g.*, Shawler et al., 2021), eco-geomorphic feedbacks between islands and their associated dunes and barrier-backbarrier marshes and lagoons (*e.g.*, Walters et al., 2014; Durán Vinent and Moore, 2015; Reeves et al., 2020), and current and future human modifications such as shore-attached breakwaters being installed along central Wallops Island and beach nourishment on Assateague and Wallops islands.

5.2.2. Sediment trapping at tidal inlets

A growing body of literature emphasizes the importance of tidal inlets in controlling barrier-island behavior. For example, in their "runaway transgression hypothesis" FitzGerald et al. (2008, 2018) posit that 1) sea-level rise drives backbarrier marsh loss and thus increases backbarrier tidal prism; 2) increased tidal prism enlarges inlet cross-sectional area and modifies transport patterns, leading to the growth of flood- and ebb-tidal delta shoals; and 3) sand sequestering in depositional landforms (*i.e.*, shoals) eventually contributes to barrier-island disintegration and/or rapid landward migration. However, a recent test of this hypothesis on the Virginia coast indicates that landward barrier migration more than compensates for backbarrier marsh loss, inhibiting tidal prism changes at most inlets (Deaton et al., 2017). However, at least Wachapreague Inlet (~42 km south of Lighthouse Ridge) has experienced a modest increase in tidal prism through time (Fenster et al., 2011) and its ebb-tidal delta may function as a trap for longshore sediment to the southernmost Virginia barrier islands (Fenster et al., 2016). This latter study highlights the role of tidal inlets as potential sinks for alongshore-transported sand. Further, in addition to ebb deltas, the formation and growth of flood-tidal deltas has also been recognized as a significant coastal sand sink (*e.g.*, Nienhuis and Ashton, 2016). Flood-tidal delta deposition can provide a platform for barrier migration (*e.g.*, Mallinson et al., 2010) and increase barrier-island resilience to drowning in response to sea-level rise (*e.g.*, Nienhuis and Lorenzo-Trueba, 2019) but can also trap sand and thus impact local barrier sediment supply (*e.g.*, Shawler et al., 2019b; Zăinescu et al., 2019).

Our data and these prior studies all highlight that inlets, through sequestration of sand in both ebb- and flood-tidal deltas, function as important controls on sand transport on barrier coasts, though the precise tidal-inlet morphodynamic response to sea-level rise likely depends on several site-specific variables. These processes are likely to be more active during periods of more frequent and/or intense storms, such as during the Medieval Climate Anomaly (*ca.* 950–1250 CE) and the Little Ice Age (*ca.* 1400–1900 CE), when both the Virginia Barrier Islands and the Outer Banks of North Carolina experienced increased inlet formation (Culver et al., 2007; Timmons et al., 2010; Mallinson et al., 2011, 2018; Raff et al., 2018). Given the likelihood of enhanced 21st century tropical and extra-tropical cyclone activity along the U.S. mid-Atlantic (Bender et al., 2010; Michaelis et al., 2017; Paerl et al., 2019), the formation of new inlets or re-breaching at former inlet locations is a realistic scenario along the Virginia coast. For example, the extratropical cyclonic Ash Wednesday (1962) storm caused breaches on northern Assateague Island (~48 km updrift Lighthouse Ridge) and recent extratropical storms have caused regular ephemeral breaching of Tom's Cove Isthmus (Seminack and McBride, 2015b; see also Fig. 2b). Data from this study indicate that the barrier-proximal portion of Tom's Cove contains potentially erodible sand and that the central portion of the embayment offers accommodation that may allow for the development of flood-tidal delta deposits. Such a scenario—similar to that associated with the formation of Cherry Tree Inlet along a narrow section of Assateague during the late 18th and early 19th centuries—would not only impact the local dynamics at Chincoteague Inlet but may also affect local (1 km) to regional (10+ km) sediment fluxes through the formation of an additional longshore transport sink. Future research and planning in Virginia and along other barrier coasts must emphasize the role and timescales of inlet formation and the growth of both ebb and flood tidal deltas on interconnectivity between updrift and downdrift barriers.

5.3. Global importance of large longshore sediment sinks

Coastal landforms such as spits, beach/foredune-ridge plains, wave-dominated deltas, strandplains, and chenier plains function as sediment traps which modify rates of alongshore sediment bypassing to downdrift coasts. Yet, the behavior (*e.g.*, progradation, erosion, stability) of these systems is also dependent on sediment supply from updrift and cross-shore sources. In other words, coastal landform formation is both a product of sediment inputs and a control on downdrift sediment supply. For example, updrift sandy headland erosion provides sufficient sediment to promote downdrift barrier elongation/progradation on the Louisiana coast (Torres et al., 2020). Likewise, the formation and stability of beach ridges on the West African coast is driven by changes in both sand source and transport patterns (Anthony, 1995). In southeastern Australia, time-varying embayment interconnectivity drives changing progradational shoreline response (Oliver et al., 2020). Similarly, sandy shoreline behavior along Santa Catarina Island in Brazil is controlled by time-varying sediment fluxes resulting from the complex interplay of headland bypassing, dune overpassing, longshore transport between and past embayed beaches, and the growth of strandplains and spits which starve downdrift coasts (Vieira da Silva, 2016a; Vieira da Silva, 2016b; Hein et al., 2019b). On the barrier-island coast of the Danish Wadden Sea, updrift coastal reconfiguration resulted in collapse of the downdrift barrier-island chain (Fruergaard et al., 2021). Along the North Carolina coast in the United States, spit growth at the Power Squadron Spit trapped 30% of longshore transport and reduced wave energy at an immediately downdrift barrier island, leading to an accelerated rate of shoreline retreat (Park and Wells, 2007); this is similar to our observations along the Virginia coast. Likewise, deposition at North Island, a spit on the South Carolina (USA) coast, captures an estimated 15% of alongshore and cross-shore sediment inputs to its coastal compartment (Wright et al., 2017). These studies and our own results emphasize the dynamic competition between longshore transport and temporary to permanent storage in complex coastal depositional landforms.

We compile examples of coastal depositional landforms and place Assateague, Chincoteague, and Wallops islands in context with these other systems (Table 6). While this list is not necessarily comprehensive, it does provide global context for this case study. The volume of sand trapped in southern Assateague (10^8 m^3) since *ca.* 1830 CE is equivalent to the large subtropical beach-ridge plains along the coasts of Brazil and Australia. Yet, the annual sand flux into Assateague is at least six times greater, an observation that largely reflects that rates of progradation are one-to-two orders of magnitude higher on most shore-parallel elongating spits, most especially southern Assateague. By contrast, cross-shore prograding barrier islands such as Chincoteague and Wallops accumulate sediment at rates similar to strandplains (10^4 m^3 yr^{-1}) and, thus, the fluxes of sediment trapped are lower than those on Assateague. The compilation demonstrates that progradational barrier islands generally trap sediment over long timescales (centuries and millennia) at annual rates similar to strandplains; notably both grow predominantly cross-shore and seaward, into generally deeper water. By contrast, the examples of spits, which largely elongate parallel to shore and thus capture sediment along their

relatively low-energy recurved ends, are much more dynamic and vary greatly in their total volumes, fluxes, and progradation rates. This observation aligns well with numerical modeling work indicating that spit morphodynamics depend on complex interactions between wave climate, updrift shoreline behavior and sediment fluxes, alongshore sediment transport gradients, and instability of the possibly highly-autogenic spit hook (Ashton et al., 2016).

These insights emphasize the importance of accounting for highly local controls (*i.e.*, sediment trapping, framework geology, changing hydrodynamics) on coastal behavior in the context of coastal management. For example, given the alongshore couplings indicated by our results, a system-wide approach to managing sediment is necessary along the Virginia coast and, by extension, other coasts worldwide. This has also been proposed for Louisiana (USA), where barrier-island restoration and management efforts have historically focused on individual islands rather than multiple barrier-backbarrier systems along the same chain (Khalil et al., 2015). Foundational science which explores the framework geology of the Virginia coast (*e.g.*, Raff et al., 2018; Brothers et al., 2020; Shawler et al., 2021) is an important first step towards improving coastal management. Indeed, similar efforts to map the shoreface in New South Wales, Australia demonstrate that increased knowledge of framework geology and improved shoreline change models together enhance coastal management and planning (Kinsela et al., 2020).

6. Conclusions

This study emphasizes the important role of natural coastal sediment sinks in the regulation of longshore transport and behavior of downdrift siliciclastic coastal systems. Through the integration of millennial-, centennial-, and decadal-scale records of coastal change recorded in progradational ridges and backbarrier deposits of the Assateague-Chincoteague-Wallops system, we demonstrate:

- The Assateague-Chincoteague-Wallops barrier-island system formed offshore of its present position >6000 years ago and underwent a multi-centennial period of net landward migration until *ca.* 2250 years ago.
- Chincoteague Island stabilized and prograded from *ca.* 2250 to 400 years ago; the rapid elongation and progradation of southern Assateague and northern Wallops began in *ca.* 1830 CE (~190 years ago).
- A phase of reduced/no progradation at southern Assateague Island from *ca.* 400 to 190 years ago coincided with updrift barrier breaching and sand sequestration in flood-tidal delta shoals.
- Chincoteague and Wallops, two progradational barrier islands, trap total volumes of sand (~10^6–10^7 m^3) at rates (~10^4 m^3 yr^{-1}) broadly similar to global examples of mainland-attached beach-ridge plains.
- Southern Assateague Island, a southerly elongating spit, traps a similar volume of sand (10^8 m^3) as compared with strandplains, but with sediment fluxes that are up to six times greater.
- Over the last 120 years, the growth of southern Assateague and Wallops islands together trapped at least 60% of longshore sediment, a process that likely starved downdrift barriers of 'beach-quality' sand and corresponds with the rapid erosion/migration ($\geq$3 m yr^{-1}) of downdrift barrier islands.
- Regional coastal planning must account for the impacts of natural coastal sediment sinks such as progradational landforms and tidal inlets that—in conjunction with forcings such as sea-level rise and storminess—establish the baseline conditions that control the behavior of sandy coastal systems.

These findings stand in direct contrast to recent work which predicts the wholesale collapse of sandy coastal features in response to sea-level rise (*e.g.*, Vousdoukas et al., 2020). Instead, this work emphasizes the importance of regional controls on sediment transport as a determinant of changes between regressive and transgressive coastal behavior.

7. Data availability

Sediment core descriptions, grain size analysis results, and editable radiocarbon and OSL tables from this study are available at: https://doi.org/10.25773/53bv-4p15.

Author credit statement

Shawler: conceptualization, methodology, funding acquisition, investigation, formal analysis, visualization, data curation, writing – original draft; **Hein:** supervision, conceptualization, methodology, funding acquisition, resources, writing -review and editing; **Obara:** investigation, visualization, formal analysis, writing -review and editing; **Robbins:** investigation, visualization, formal analysis, writing - review and editing; **Huot:** investigation, visualization, formal analysis, writing – review and editing; **Fenster**: conceptualization, methodology, funding acquisition, resources, investigation, writing - review and editing.

Declaration of competing interest

The authors declare that they have no known competing financial interests or personal relationships that could have appeared to influence the work reported in this paper.

Acknowledgements

This research was supported by funds from the Commonwealth of Virginia and the Virginia Center for Innovative Technology. This paper was prepared by Justin Shawler using Federal funds under NOAA award number NA18OAR4170083, Virginia Sea Grant College Program Project #721557, from the National Oceanic and Atmospheric Administration's (NOAA) National Sea Grant College Program, U.S. Department of Commerce. The statements, findings, conclusions, and recommendations are those of the author(s) and do not necessarily reflect the views of the Commonwealth of Virginia, Virginia Center for Innovative Technology, Virginia Sea Grant, NOAA, or the U.S. Department of Commerce. We thank the following people for assistance with field data collection and fruitful field discussions: Dr. Daniel Ciarletta, Kate DeMarco, Dr. Ioannis Georgiou, Dr. John Harding, Lauren Herbine, Loren Mayr, Kaite McPherran, Colleen Scott, Dr. Christopher Seminack, and Jake Tidwell. We especially thank Jennifer Connell for field and laboratory assistance. We thank Andrea Bautista for laboratory assistance with OSL analyses. For logistical support, we thank the Virginia Institute of Marine Science Eastern Shore Lab team including Dr. Richard Snyder, Sean Fate, Edward Smith, P.G. Ross, Justin Paul, Glenn Brundage, and Linda Ward. We thank numerous private homeowners and businesses, the Town of Chincoteague (and especially Chincoteague Town Manager Jim West [retired]), NASA Wallops, and Chincoteague National Wildlife Refuge (special use permit numbers: 2017–008, 2019–002, and 2021–001) for access, sampling, and coring permissions. This paper is Contribution No. 4034 of the Virginia Institute of Marine Science, William & Mary.

Appendix A. Supplementary data

Supplementary data to this article can be found online at

https://doi.org/10.1016/j.quascirev.2021.107096.

References

American Shore and Beach Preservation Association (ASBPA), 2020. Beach nourishment database. Retrieved from. https://gim2.aptim.com/ASBPANationwideRenourishment/.

Anderson, J.B., Wallace, D.J., Simms, A.R., Rodriguez, A.B., Weight, R.W.R., Taha, Z.P., 2016. Recycling sediments between source and sink during a eustatic cycle: systems of late Quaternary northwestern Gulf of Mexico Basin. Earth Sci. Rev. 153, 111–138.

Anthony, E.J., 1995. Beach-ridge development and sediment supply: examples from West Africa. Mar. Geol. 129, 175–186.

Anthony, E.J., 2015. Patterns of Sand Spit Development and Their Management Implications on Deltaic, Drift-Aligned Coasts: the Cases of the Senegal and Volta River Delta Spits, West Africa. Coastal Research Library, pp. 21–36.

Armstrong, S.B., Lazarus, E.D., 2019. Masked shoreline erosion at large spatial scales as a collective effect of beach nourishment. Earth's Fut. 7, 74–84.

Ashton, A.D., Nienhuis, J., Ells, K., 2016. On a neck, on a spit: controls on the shape of free spits. Earth Surf. Dyn. 4, 193–210.

Aubrey, D.G., Gaines, A.G., 1982. Rapid formation and degradation of barrier spits in areas with low rates of littoral drift. Mar. Geol. 49, 257–277.

Belknap, D.F., Kraft, J.C., 1985. Influence of antecedent geology on stratigraphic preservation potential and evolution of Delaware's barrier systems. Mar. Geol. 63, 235–262.

Bender, M.A., Knutson, T.R., Tuleya, R.E., Sirutis, J.J., Vecchi, G.A., Garner, S.T., Held, I.M., 2010. Modeled impact of anthropogenic warming on the frequency of intense Atlantic hurricanes. Science 327, 454–458, 80.

Beudin, A., Ganju, N.K., Defne, Z., Aretxabaleta, A.L., 2017. Physical response of a back-barrier estuary to a post-tropical cyclone. J. Geophys. Res. Ocean. 122, 5888–5904.

Billy, J., Robin, N., Hein, C.J., FitzGerald, D.M., Certain, R., 2018. Impact of relative sea-level changes since the last deglaciation on the formation of a composite paraglacial barrier. Mar. Geol. 400, 76–93.

Boon, J.D., Mitchell, M., 2015. Nonlinear change in sea level observed at North American tide stations. J. Coast Res. 31, 1295–1305.

Brenner, O.T., Moore, L.J., Murray, A.B., 2015. The complex influences of back-barrier deposition, substrate slope and underlying stratigraphy in barrier island response to sea-level rise: Insights from the Virginia Barrier Islands, Mid-Atlantic Bight, U.S.A. Geomorphology 246, 334–350.

Bristow, C.S., Pucillo, K., 2006. Quantifying rates of coastal progradation from sediment volume using GPR and OSL: The Holocene fill of Guichen Bay, southeast South Australia. Sedimentology 53, 769–788.

Bronk Ramsey, C., 2009. Bayesian analysis of radiocarbon dates. Radiocarbon 51, 337–360.

Brothers, L.L., Foster, D.S., Pendleton, E.A., Baldwin, W.E., 2020. Seismic stratigraphic framework of the continental shelf o ff shore Delmarva, U.S.A.: Implications for Mid-Atlantic Bight Evolution since the Pliocene. Mar. Geol. 428, 106287.

Byrnes, M.R., 1988. Holocene Geology and Migration of a Low-Profile Barrier Island System, Metompkin Island, Virginia. ProQuest Diss. Theses, p. 422.

Campbell, T.J., Benedet, L., 2006. Beach nourishment magnitudes and trends in the U.S. J. Coast Res. 57–64.

Carruthers, E.A., Lane, D.P., Evans, R.L., Donnelly, J.P., Ashton, A.D., 2013. Quantifying overwash flux in barrier systems: An example from Martha's Vineyard, Massachusetts, USA. Mar. Geol. 343, 15–28.

Carter, R.W.G., 1986. The morphodynamics of beach-ridge formation: Magilligan, Northern Ireland. Mar. Geol. 73, 191–214.

Ciarletta, D.J., Lorenzo-Trueba, J., Ashton, A.D., 2019a. Mechanism for retreating barriers to autogenically form periodic deposits on continental shelves. Geology 47, 1–4.

Ciarletta, D.J., Shawler, J.L., Tenebruso, C., Hein, C.J., Lorenzo-Trueba, J., 2019b. Reconstructing coastal sediment budgets from beach- and foredune-ridge morphology: A coupled field and modeling approach. J. Geophys. Res. Earth Surf. 1398–1416.

Ciarletta, D.J., Miselis, J.L., Shawler, J.L., Hein, C.J., 2021. Quantifying thresholds of barrier geomorphic change in a cross-shore sediment-partitioning model. Earth Surf. Dyn. 9, 183–203.

Cowell, P.J., Kinsela, M.A., 2018. Shoreface controls on barrier evolution and shoreline change. Barrier Dynamics and Response to Changing Climate. Springer, pp. 243–275.

Culver, S.J., Grand Pre, C.A., Mallinson, D.J., Riggs, S.R., Corbett, D.R., Foley, J., Hale, M., Metger, L., Ricardo, J., Rosenberger, J., Smith, C.G., Smith, C.W., Snyder, S.W., Twamley, D., Farrell, K.M., Horton, B.P., 2007. Late Holocene barrier island collapse. Sediment. Rec. 5, 4–8.

Curray, J.R., 1964. Transgression and regression. In: Miller, R.L. (Ed.), Papers in Marine Geology. MacMillan, New York, pp. 175–203.

Deaton, C.D., Hein, C.J., Kirwan, M.L., 2017. Barrier island migration dominates ecogeomorphic feedbacks and drives salt marsh loss along the Virginia Atlantic Coast, USA. Geology 45, 123–126.

Durán Vinent, O., Moore, L.J., 2015. Barrier island bistability induced by biophysical interactions. Nat. Clim. Change 5, 158–162.

Eisemann, E.R., Wallace, D.J., Buijsman, M.C., Pierce, T., 2018. Response of a vulnerable barrier island to multi-year storm impacts: LiDAR-data-inferred morphodynamic changes on Ship Island, Mississippi, USA. Geomorphology 313, 58–71.

Elko, N., Briggs, T.R., Benedet, L., Robertson, Q., Thomson, G., Webb, B.M., Garvey, K., 2021. A century of U.S. beach nourishment. Ocean Coast Manag. 199, 105406.

Elliott, E.A., McKee, B.A., Rodriguez, A.B., 2015. The utility of estuarine settling basins for constructing multi-decadal, high-resolution records of sedimentation. Estuar. Coast Shelf Sci. 164, 105–114.

Ells, K., Brad Murray, A., 2012. Long-term, non-local coastline responses to local shoreline stabilization. Geophys. Res. Lett. 39, 1–7.

Emery, A.R., Hodgson, D.M., Barlow, N.L.M., Carrivick, J.L., Cotterill, C.J., Mellett, C.L., Booth, A.D., 2019. Topographic and hydrodynamic controls on barrier retreat and preservation: An example from Dogger Bank, North Sea. Mar. Geol. 416, 105981.

Engelhart, S.E., Horton, B.P., 2012. Holocene sea level database for the Atlantic coast of the United States. Quat. Sci. Rev. 54, 12–25.

Fenster, M.S., McBride, R.A., Trembanis, A., Richardson, T., Nebel, S.H., 2011. A field test of the theoretical evolution of a mixed-energy barrier coast to a regime of accelerated sea-level rise. Proc. Coast. Sediments 2011, 216–229.

Fenster, M.S., Bundick, J.A., McBride, R.A., Fenster, M.S., Seminack, C.T., Richardson, T.M., Sepanik, J.M., Hanley, J.T., Bundick, J.A., Tedder, E., 2015a. Morphodynamics of Wallops Island, Virginia: A mixed-energy, human-modified barrier island. In: Brezinski, D.K., Halka, J.P., Ortt, J., A, R. (Eds.), Holocene Barrier-Island Geology and Morphodynamics of the Maryland and Virginia Open-Ocean Coasts: Fenwick, Assateague, Chincoteague, Wallops, Cedar, and Parramore Islands, Tripping from the Fall Line: Field Excursions for the GSA Annual Meeting, Baltimore, 2015: Geological Society of America Field Guide 40, vol. 40. Geological Society of America, pp. 358–370.

Fenster, M.S., McBride, R.A., McBride, R.A., Fenster, M.S., Seminack, C.T., Richardson, T.M., Sepanik, J.M., Hanley, J.T., Bundick, J.A., Tedder, E., 2015b. Barrier-island geology and morphodynamics along the open-ocean coast of the Delmarva Peninsula: An Overview. In: Brezinski, D.K., Halka, J.P., Ortt, J., A, R. (Eds.), Holocene Barrier-Island Geology and Morphodynamics of the Maryland and Virginia Open-Ocean Coasts: Fenwick, Assateague, Chincoteague, Wallops, Cedar, and Parramore Islands, Tripping from the Fall Line: Field Excursions for the GSA Annual Meeting, Baltimore, 2015: Geological Society of America Field Guide 40, vol. 40. Geological Society of America, pp. 310–334.

Fenster, M., Dolan, R., 1996. Assessing the impact of tidal inlets on adjacent barrier island shorelines. J. Coast. Res. 12, 294–310.

Fenster, M.S., Dolan, R., Smith, J.J., 2016. Grain-size distributions and coastal morphodynamics along the southern Maryland and Virginia barrier islands. Sedimentology 63, 809–823.

Finkelstein, K., Ferland, M.A., 1987. Back-barrier response to sea-level rise, Eastern Shore of Virginia. In: Nummedal, D., Pilkey, O.H., Howard, J. (Eds.), Sea-Level Fluctuations and Coastal Evolution, vol. 41. SEPM (Society for Sedimentary Geology), pp. 145–155.

FitzGerald, D.M., 1984. Interactions between the ebb-tidal delta and landward shoreline: Price Inlet, South Carolina. J. Sediment. Res. 54, 1303–1318.

FitzGerald, D.M., Cleary, W.J., Buynevich, I.V., Hein, C.J., Klein, A.H.F., Asp, N., Angulo, R., Fitzgerald, D.M., Cleary, W.J., Buynevich, I.V., Hein, C.J., Klein, A.H.F., Asp, N., Angulo, R., 2007. Strandplain Evolution along the Southern Coast of Santa Catarina, Brazil. J. Coast Res. 152–156.

FitzGerald, D.M., Fenster, M.S., Argow, B.A., Buynevich, I.V., 2008. Coastal impacts due to sea-level rise. Annu. Rev. Earth Planet Sci. 36, 601–647.

FitzGerald, D.M., Hein, C.J., Hughes, Z., Kulp, M., Georgiou, I., Miner, M., 2018. Runaway Barrier Island Transgression Concept: Global Case Studies. In: Moore, L.J., Murray, A.B. (Eds.), Barrier Dynamics and Response to Changing Climate. Springer International Publishing, Cham, pp. 3–56.

Fruergaard, M., Andersen, T.J., Johannessen, P.N., Nielsen, L.H., Pejrup, M., 2013. Major coastal impact induced by a 1000-year storm event. Sci. Rep. 3, 1–7.

Fruergaard, M., Kirkegaard, L., Østergaard, A.T., Murray, A.S., Andersen, T.J., 2019. Dune ridge progradation resulting from updrift coastal reconfiguration and increased littoral drift. Geomorphology 330, 69–80.

Fruergaard, M., Sander, L., Goslin, J., Andersen, T.J., 2021. Temporary late Holocene barrier-chain deterioration due to insufficient sediment availability, Wadden Sea, Denmark. Geology 49, 162–167.

Gal, N.S., Wallace, D.J., Miner, M.D., Hollis, R.J., Dike, C., Flocks, J.G., 2021. Influence of antecedent geology on the Holocene formation and evolution of Horn Island, Mississippi, USA. Mar. Geol. 431, 106375.

Garel, E., Sousa, C., Ferreira, Ó., Morales, J.A., 2014. Decadal morphological response of an ebb-tidal delta and down-drift beach to artificial breaching and inlet stabilisation. Geomorphology 216, 13–25.

Goettle, M.S., 1978. Geological Development of the Southern Portion of Assateague Island. M.S. Thesis. University of Delaware, Virginia.

Hall, M.J., Pilkey, O.H., 1991. Effects of Hard Stabilization on Dry Beach Width for New-Jersey. J. Coast Res. 7, 771–785.

Halsey, S., 1978. Late Quaternary Geologic History and Morphologic Development of the Barrier Island System along the Delmarva Peninsula of the Mid-Atlantic Bight. PhD Thesis. University of Delaware.

Hapke, C.J., Himmelstoss, E.a., Kratzmann, M., List, J.H., Thieler, E.R., 2010. National Assessment of Shoreline Change: Historical Shoreline Change along the New England and Mid-Atlantic Coasts Open-File Report 2010 – 1118, p. 57.

Hapke, C.J., Kratzmann, M.G., Himmelstoss, E.A., 2013. Geomorphic and human influence on large-scale coastal change. Geomorphology 199, 160–170.

Hapke, C.J., Plant, N.G., Henderson, R.E., Schwab, W.C., Nelson, T.R., 2016. Decoupling processes and scales of shoreline morphodynamics. Mar. Geol. 381, 42–53.

Hayden, B.P., Hayden, N.R., 2003. Decadal and century-long changes in storminess

at long-term ecological research sites. In: Greenland, D., Goodin, D.G., Smith, R.S. (Eds.), Climate Variability and Ecosystem Response at Long-Term Ecological Research Sites. Oxford University Press, New York, pp. 262–285.
Headland, J.R., Vallianos, L., Sheldon, J.G., 1987. Coastal processes at Wallops Island, Virginia. In: In: Proceedings, Coastal Sediments '87, New Orleans, LA, pp. 1305–1320.
Heaton, T.J., Köhler, P., Butzin, M., Bard, E., Reimer, R.W., Austin, W.E.N., Bronk Ramsey, C., Grootes, P.M., Hughen, K.A., Kromer, B., Reimer, P.J., Adkins, J., Burke, A., Cook, M.S., Olsen, J., Skinner, L.C., 2020. Marine20 - The Marine Radiocarbon Age Calibration Curve (0-55,000 cal BP). Radiocarbon 62, 779–820.
Hein, C.J., FitzGerald, D.M., Cleary, W.J., Albernaz, M.B., De Menezes, J.T., Klein, A.H.d.F., 2013. Evidence for a transgressive barrier within a regressive strandplain system: Implications for complex coastal response to environmental change. Sedimentology 60, 469–502.
Hein, C.J., FitzGerald, D.M., Buynevich, I.V., Heteren, S.V.A.N., Kelley, J.T., 2014a. Evolution of paraglacial coasts in response to changes in fluvial sediment supply. Geol. Soc. London, Spec. Publ. 388, 247–280.
Hein, C.J., FitzGerald, D.M., de Menezes, J.T., Cleary, W.J., Klein, A.H.F., Albernaz, M.B., 2014b. Coastal response to late-stage transgression and sea-level highstand. Bull. Geol. Soc. Am. 126, 459–480.
Hein, C.J., FitzGerald, D.M., de Souza, L.H.P., Georgiou, I.Y., Buynevich, I.V., Klein, A.H. da F., de Menezes, J.T., Cleary, W.J., Scolaro, T.L., 2016. Complex coastal change in response to autogenic basin infilling: An example from a sub-tropical Holocene strandplain. Sedimentology 63, 1362–1395.
Hein, C.J., Georgiou, I.Y., FitzGerald, D.M., De Souza, L.H.P., Klein, A.H.F., de Menezes, J.T., 2015. Wave energy, sediment supply, and sea-level fall: Late Holocene basin infilling in southern Brazil. In: The Proceedings of the Coastal Sediments 2015, vols. 1–16. WORLD SCIENTIFIC.
Hein, C.J., Fallon, A.R., Rosen, P., Hoagland, P., Georgiou, I.Y., FitzGerald, D.M., Morris, M., Baker, S., Marino, G.B., Fitzsimons, G., 2019a. Shoreline Dynamics Along a Developed River Mouth Barrier Island: Multi-Decadal Cycles of Erosion and Event-Driven Mitigation. Front. Earth Sci. 7, 1–23.
Hein, C.J., Shawler, J.L., De Camargo, J.M., Klein, A.H.d.F., Tenebruso, C., Fenster, M.S., 2019b. The role of coastal sediment sinks in modifying longshore sand fluxes: Examples from the coasts of southern Brazil and the Mid-Atlantic USA. Coastal Sediments 2019. World Scientific, pp. 2330–2344.
Hein, C.J., Ashton, A.D., 2020. Long-term shoreline morphodynamics: processes and preservation of environmental signals. Sandy Beach Morphodynamics. Elsevier, pp. 487–531.
Hequette, A., Ruz, M.-H., 1991. Spit and barrier island migration in the southeastern Canadian Beaufort Sea. J. Coast Res. 7, 677–698.
Hill, P.R., 1990. Coastal geology of the King Point area, Yukon Territory, Canada. Mar. Geol. 91, 93–111.
Hine, A.C., 1979. Mechanisms of berm development and resulting beach growth along a barrier spit complex. Sedimentology 26, 333–351.
Hoan, L.X., Hanson, H., Larson, M., Kato, S., 2011. A mathematical model of spit growth and barrier elongation: Application to Fire Island Inlet (USA) and Badreveln Spit (Sweden). Estuar. Coast Shelf Sci. 93, 468–477.
Hollis, R.J., Wallace, D.J., Miner, M.D., Gal, N.S., Dike, C., Flocks, J.G., 2019. Late Quaternary evolution and stratigraphic framework influence on coastal systems along the north-central Gulf of Mexico, USA. Quat. Sci. Rev. 223, 105910.
Houser, C., Hapke, C., Hamilton, S., 2008. Controls on coastal dune morphology, shoreline erosion and barrier island response to extreme storms. Geomorphology 100, 223–240.
Jarrett, J.T., 1976. Tidal Prism - Inlet Area Relationships. U.S. Army Engineer Waterways Experiment Station.
Jones, M., 2016. Considering Holistic Coastal Response to Climate-Change Induced Shifts in Natural Processes and Anthropogenic Modifications. University of North Carolina, Chapel Hill.
Kang, X., Xia, M., Pitula, J.S., Chigbu, P., 2017. Dynamics of water and salt exchange at Maryland Coastal Bays. Estuar. Coast Shelf Sci. 189, 1–16.
Kelley, J.T., Belknap, D.F., Walsh, J.A., 2015. Tidal flat-barrier spit interactions in a fetch-limited, macro-tidal embayment, Lubec, Maine, USA. Sand and Gravel Spits. Springer, pp. 195–216.
Khalil, S.M., Raynie, R.C., 2015. An Integrated System-Based Approach To Restoration Of Louisiana's Barrier Islands. The Proceedings of the Coastal Sediments 2015. World Scientific, L, p. 14.
King Jr., D.B., Ward, D.L., Hudgins, M.H., Williams, G.G., 2011. Storm Damage Reduction Project Design for Wallops Island, Virginia, Version 1.01. *Engineer Research and Development Center, Vicksburg, Mississippi, U.S.* Army Corps Eng. 197. Report No. ERDC/LAB TR-11-9.
Kinsela, M.A., Hanslow, D.J., Carvalho, R.C., Linklater, M., Ingleton, T.C., Morris, B.D., Allen, K.M., Sutherland, M.D., Woodroffe, C.D., 2020. Mapping the Shoreface of Coastal Sediment Compartments to Improve Shoreline Change Forecasts in New South Wales, Australia. Estuar. Coast. https://doi.org/10.1007/s12237-020-00756-7.
Komar, P.D., Allan, J.C., 2008. Increasing hurricane-generated wave heights along the U.S. East Coast and their climate controls. J. Coast Res. 24, 479–488.
Krantz, D.E., Hobbs, C.H., Wikel, G.L., Krantz, D.E., Wikel, G.L., 2016. Atlantic coast and inner shelf. In: Bailey, C.M., Sherwood, W.C., Eaton, L.S., Powards, D.S. (Eds.), Geology of Virginia. Virginia Museum of Natural History, pp. 341–380.
Kraus, N.C., Galgano, F.A., 2001. Beach Erosional Hot Spots: Types, Causes, and Solutions. Engineer Research and Development Center. U.S. Army Corps of Engineers, Coastal and Hydraulics Laboratory, Vicksburg, Mississippi.
Laïbi, R.A., Anthony, E.J., Almar, R., Castelle, B., Senechal, N., Kestenare, E., 2014. Longshore drift cell development on the human-impacted Bight of Benin sand barrier coast, West Africa. J. Coast Res. 70, 78–83.
Lazarus, E.D., Goldstein, E.B., 2019. Is There a Bulldozer in your Model? J. Geophys. Res. Earth Surf. 124, 696–699.
Leatherman, S.P., 1979. Migration of Assateague Island, Maryland, by inlet and overwash processes. Geology 7, 104.
Lorenzo-Trueba, J., Ashton, A.D., 2014. Rollover, drowning, and discontinuous retreat: Distinct modes of barrier response to sea-level rise arising from a simple morphodynamic model. J. Geophys. Res. Earth Surf. 119, 779–801.
Mallinson, D.J., Smith, C.W., Culver, S.J., Riggs, S.R., Ames, D., 2010. Geological characteristics and spatial distribution of paleo-inlet channels beneath the outer banks barrier islands, North Carolina, USA. Estuar. Coast Shelf Sci. 88, 175–189.
Mallinson, D.J., Smith, C.W., Mahan, S., Culver, S.J., McDowell, K., 2011. Barrier island response to late Holocene climate events, North Carolina, USA. Quat. Res. 76, 46–57.
Mallinson, D.J., Culver, S.J., Leorri, E., Mitra, S., Mulligan, R., Riggs, S.R., 2018. Barrier island and estuary co-evolution in response to Holocene climate and sea-level change: Pamlico Sound and the Outer Banks barrier islands, North Carolina, USA. In: Moore, L.J., Murray, A.B. (Eds.), Barrier Dynamics and Response to Changing Climate. Springer International Publishing, Cham, p. 395.
Masselink, G., Van Heteren, S., 2014. Response of wave-dominated and mixed-energy barriers to storms. Mar. Geol. 352, 321–347.
McPherran, K., Dohner, S., Trembanis, A., 2021. A comparison of the temporal evolution of hydrodynamics and inlet morphology during Tropical Storm Fay (2020). Shore Beach 89, 11–22.
Michaelis, A.C., Willison, J., Lackmann, G.M., Robinson, W.A., 2017. Changes in winter North Atlantic extratropical cyclones in high-resolution regional pseudo-global warming simulations. J. Clim. 30, 6905–6925.
Milne, G.A., Gehrels, W.R., Hughes, C.W., Tamisiea, M.E., 2009. Identifying the causes of sea-level change. Nat. Geosci. 2, 471–478.
Miselis, J.L., Lorenzo-Trueba, J., 2017. Natural and human-induced variability in barrier-island response to sea level rise. Geophys. Res. Lett. 44, 11,922–11,931.
Mixon, R.B., 1985. Stratigraphic and geomorphic framework of uppermost Cenozoic deposits in the southern Delmarva Peninsula, Virginia and Maryland. U. S. Geol. Surv. Prof. Pap. 1067 (G), 53.
Montello, T.M., FitzGerald, D.M., van Heteren, S., Caldwell, D.W., Fink, L.K., 1992. Stratigraphy and evolution of the barrier system along the Wells-Ogunquit embayment in southern Maine. Boston Univ. Coast. Envir. Res. Group Tech. Rept. 15, 220.
Moore, L.J., List, J.H., Williams, S.J., Stolper, D., 2010. Complexities in barrier island response to sea level rise: Insights from numerical model experiments, North Carolina Outer Banks. J. Geophys. Res. 115, F03004.
Morton, R.A., 2008. Historical changes in the Mississippi-Alabama barrier-island chain and the roles of extreme storms, sea level, and human activities. J. Coast Res. 24, 1587–1600.
Murray, A.S., Wintle, A.G., 2000. Luminescence dating of quartz using an improved single-aliquot regenerative-dose protocol. Radiat. Meas. 32, 57–73.
Murray, A.S., Wintle, A.G., 2003. The single aliquot regenerative dose protocol: potential for improvements in reliability. Radiat. Meas. 37, 377–381.
National Aeronautics and Space Administration, 2019. Final NASA WFF Shoreline Enhancement and Restoration Project Environmental Assessment, p. 84.
Naumann, M., Lampe, R., Hoffmann, G., 2009. Coastal evolution of a Holocene barrier spit (Bug peninsula/NW-Rügen) deduced from geological structure and relative sea-level. Quat. Sci. J. 58, 164–173.
Nebel, S.H., Trembanis, A.C., Barber, D.C., 2012. Shoreline Analysis and Barrier Island Dynamics: Decadal Scale Patterns from Cedar Island, Virginia. J. Coast Res. 280, 332–341.
Nielsen, S.T., Clemmensen, L.B., Andreasen, F., 1995. The middle and late Holocene barrier spit system at Vejers, Denmark: structure and development. Bull. Geol. Soc. Den. 42, 105–119.
Nienhuis, J.H., Ashton, A.D., 2016. Mechanics and rates of tidal inlet migration: Modeling and application to natural examples. J. Geophys. Res. Earth Surf. 121, 2118–2139.
Nienhuis, J.H., Lorenzo-Trueba, J., 2019. Can Barrier Islands Survive Sea-Level Rise? Quantifying the Relative Role of Tidal Inlets and Overwash Deposition. Geophys. Res. Lett. 46, 14613–14621.
Nooren, K., Hoek, W., Winkels, T., Huizinga, A., Van Der Plicht, H., Van Dam, R.L., Van Heteren, S., Van Bergen, M.J., Prins, M.A., Reimann, T., Wallinga, J., Cohen, K.M., Minderhoud, P., Middelkoop, H., 2017. The Usumacinta-Grijalva beach-ridge plain in southern Mexico: A high-resolution archive of river discharge and precipitation. Earth Surf. Dyn. 5, 529–556.
Oliver, T.S., Dougherty, A.J., Gliganic, L.A., Woodroffe, C.D., 2015. Towards more robust chronologies of coastal progradation: Optically stimulated luminescence ages for the coastal plain at Moruya, south-eastern Australia. Holocene 25, 536–546.
Oliver, T.S., Murray-Wallace, C.V., Woodroffe, C.D., 2019a. Holocene shoreline progradation and coastal evolution at Guichen and Rivoli Bays, southern Australia. Holocene. https://doi.org/10.1177/0959683619875815.
Oliver, T.S.N., Tamura, T., Short, A.D., Woodroffe, C.D., 2019b. Rapid shoreline progradation followed by vertical foredune building at Pedro Beach, southeastern Australia. Earth Surf. Process. Landforms 44, 655–666.
Oliver, T.S.N., Tamura, T., Brooke, B.P., Short, A.D., Kinsela, M.A., Woodroffe, C.D., Thom, B.G., 2020. Holocene evolution of the wave-dominated embayed Moruya

coastline, southeastern Australia: Sediment sources, transport rates and alongshore interconnectivity. Quat. Sci. Rev. 247, 106566.
Otvos, E.G., Carter, G.A., 2013. Regressive and transgressive barrier islands on the North-Central Gulf Coast - Contrasts in evolution, sediment delivery, and island vulnerability. Geomorphology 198, 1–19.
Paerl, H.W., Hall, N.S., Hounshell, A.G., Luettich, R.A., Rossignol, K.L., Osburn, C.L., Bales, J., 2019. Recent increase in catastrophic tropical cyclone flooding in coastal North Carolina, USA: Long-term observations suggest a regime shift. Sci. Rep. 9, 1–9.
Park, J.-Y., Wells, J.T., 2007. Spit growth and downdrift erosion: Results of longshore transport modeling and morphologic analysis at the Cape Lookout cuspate foreland. J. Coast Res. 233, 553–568.
Pendleton, E.A., Brothers, L.L., Thieler, E.R., Sweeney, E.M., 2017. Sand ridge morphology and bedform migration patterns derived from bathymetry and backscatter on the inner-continental shelf offshore of Assateague Island, USA. Continent. Shelf Res. 144, 80–97.
Psuty, N.P., 2004. The Coastal Foredune: A Morphological Basis for Regional Coastal Dune Development. In: Martinez, M.L., Psuty), N.P. (Eds.), Coastal Dunes: Ecology and Conservation (Ecological Studies), 171. Springer, Berlin, Heidelberg, pp. 11–27.
Raff, J.L., Shawler, J.L., Ciarletta, D.J., Hein, E.A., Lorenzo-Trueba, J., Hein, C.J., 2018. Insights into barrier-island stability derived from transgressive/regressive state changes of Parramore Island, Virginia. Mar. Geol. 403, 1–19.
Ramsey, K.W., 2010. Stratigraphy, Correlation, and Depositional Environments of the Middle to Late Pleistocene Interglacial Deposits of Southern Delaware. Newark, DE, p. 50.
Reeves, I.R.B., Moore, L.J., Goldstein, E.B., Murray, A.B., Carr, J.A., Kirwan, M.L., 2020. Impacts of Seagrass Dynamics on the Coupled Long-Term Evolution of Barrier-Marsh-Bay Systems. J. Geophys. Res. Biogeosci. 125, 1–19.
Reimer, P.J., Austin, W.E.N., Bard, E., Bayliss, A., Blackwell, P.G., Bronk Ramsey, C., Butzin, M., Cheng, H., Edwards, R.L., Friedrich, M., Grootes, P.M., Guilderson, T.P., Hajdas, I., Heaton, T.J., Hogg, A.G., Hughen, K.A., Kromer, B., Manning, S.W., Muscheler, R., Palmer, J.G., Pearson, C., Van Der Plicht, J., Reimer, R.W., Richards, D.A., Scott, E.M., Southon, J.R., Turney, C.S.M., Wacker, L., Adolphi, F., Büntgen, U., Capano, M., Fahrni, S.M., Fogtmann-Schulz, A., Friedrich, R., Köhler, P., Kudsk, S., Miyake, F., Olsen, J., Reinig, F., Sakamoto, M., Sookdeo, A., Talamo, S., 2020. The IntCal20 Northern Hemisphere Radiocarbon Age Calibration Curve (0-55 cal kBP). Radiocarbon 62, 725–757.
Rice, T.E., Leatherman, S.P., 1983. Barrier island dynamics: The Eastern Shore of Virginia. SE. Geol. 24, 125–137.
Rick, T.C., Henkes, G.A., Lowery, D.L., Colman, S.M., Culleton, B.J., 2012. Marine radiocarbon reservoir corrections (ΔR) for Chesapeake Bay and the Middle Atlantic Coast of North America. Quat. Res. 77, 205–210.
Richter, D., Richter, A., Dornich, K., 2015. Lexsyg smart - A luminescence detection system for dosimetry, material research and dating application. Geochronometria 42, 202–209.
Robin, N., Levoy, F., Anthony, E.J., Monfort, O., 2020. Sand spit dynamics in a large tidal-range environment: insight from multiple LiDAR, UAV and hydrodynamic measurements on multiple spit hook development, breaching, reconstruction, and shoreline changes. Earth Surf. Process. Landforms. https://doi.org/10.1002/esp.4924.
Rodriguez, A.B., Fassell, M.L., Anderson, J.B., 2001. Variations in shoreface progradation and ravinement along the Texas coast, Gulf of Mexico. Sedimentology 48, 837–853.
Rodriguez, A.B., McKee, B.A., Miller, C.B., Bost, M.C., Atencio, A.N., 2020. Coastal sedimentation across North America doubled in the 20th century despite river dams. Nat. Commun. 11, 1–9.
Sangree, J.B., Widmier, J.M., 1979. Interpretation of depositional facies from seismic data. Geophysics 44, 131–160.
Seminack, C.T., McBride, R.A., McBride, R.A., Fenster, M.S., Seminack, C.T., Richardson, T.M., Sepanik, J.M., Hanley, J.T., Bundick, J.A., Tedder, E., 2015. Coastal morphodynamics of Ocean City Inlet, Maryland; Assateague Island, Maryland-Virginia; and Chincoteague Island, Virginia. In: Brezinski, D.K., Halka, J.P., Ortt, J., A, R. (Eds.), Holocene Barrier-Island Geology and Morphodynamics of the Maryland and Virginia Open-Ocean Coasts: Fenwick, Assateague, Chincoteague, Wallops, Cedar, and Parramore Islands, Tripping from the Fall Line: Field Excursions for the GSA Annual Meeting, Baltimore, 2015: Geological Society of America Field Guide 40, vol. 40. Geological Society of America, pp. 310–334.
Seminack, C.T., McBride, R.A., 2015. Geomorphic History and Diagnostic Features of Former Tidal Inlets along Assateague Island, Maryland-Virginia: A Life-Cycle Model for Inlets along Wave-Dominated Barrier Islands.
Seminack, C.T., McBride, R.A., 2019. New perspectives on the geomorphic, sedimentologic, and stratigraphic signatures of former wave-dominated tidal inlets: Assateague Island, Maryland, U.S.A. J. Sediment. Res. 89, 312–334.
Shawler, J.L., Hein, C.J., Canuel, E.A., Kaste, J.M., Fitzsimons, G.G., Georgiou, I.Y., Willard, D.A., 2019a. Tidal erosion and upstream sediment trapping modulate records of land-use change in a formerly glaciated New England estuary. Anthr. Coasts 2, 340–361.
Shawler, J.L., Ciarletta, D.J., Lorenzo-Trueba, J., Hein, C.J., 2019b. Drowned foredune ridges as evidence of pre- historical barrier-island state changes between migration and progradation. In: Coastal Sediments 2019. World Scientific, pp. 158–171.
Shawler, J.L., Ciarletta, D.J., Connell, J.E., Boggs, B.Q., Lorenzo-Trueba, J., Hein, C.J., 2021. Relative influence of antecedent topography and sea-level rise on barrier-island migration. Sedimentol. Sed 12798.
Silva, A.P., Vieira, G., Strauss, D., Murray, T., Woortmann, L.G., Taber, J., Cartwright, N., Tomlinson, R., 2021. Science of the Total Environment Headland bypassing timescales : Processes and driving forces. Sci. Total Environ. 793, 148591.
Soons, J.M., Shulmeister, J., Holt, S., 1997. The Holocene evolution of a well nourished gravelly barrier and lagoon complex, Kaitorete "Spit", Canterbury, New Zealand. Mar. Geol. 138, 69–90.
Stéphan, P., Suanez, S., Fichaut, B., 2012. Long-term morphodynamic evolution of the Sillon de Talbert gravel barrier spit, Brittany, France. Shore Beach 80, 19.
Swift, D.J.P., 1975. Barrier-island genesis: Evidence from the central Atlantic shelf, eastern U.S.A. Sediment. Geol. 14, 1–43.
Syvitski, J.P.M., Vörösmarty, C.J., Kettner, A.J., Green, P., 2005. Impact of Humans on the Flux of Terrestrial Sediment to the Global Coastal Ocean. Science 308, 376–380.
Timmons, E.A., Rodriguez, A.B., Mattheus, C.R., DeWitt, R., 2010. Transition of a regressive to a transgressive barrier island due to back-barrier erosion, increased storminess, and low sediment supply: Bogue Banks, North Carolina, USA. Mar. Geol. 278, 100–114.
Torres, J., Kulp, M., FitzGerald, D., Georgiou, I., Lepper, K., 2020. Geomorphic and temporal evolution of a Mississippi delta flanking barrier island: Grand Isle, LA. Mar. Geol. 430, 106341.
Toscano, M.A., Kerhin, R.T., York, L.L., Cronin, T.M., Williams, S.J., 1989. Quaternary stratigraphy of the inner continental shelf of Maryland. Rep. Investig. 50, 117.
U.S. Coast Survey, 1880. Navigation Chart of Green Run to Chincoteague. https://historicalcharts.noaa.gov/image=CP1556C.
US Coast & Geodetic Survey, 1910. From Isle of Wight to Chincoteague Inlet. https://historicalcharts.noaa.gov/image=LC00128_01_1910.
U.S. Geological Survey (USGS, 2016. Topobathymetric Model for Chesapeake Bay Region - District of Columbia, States of Delaware, Maryland, Pennsylvania, and Virginia, 1859 to 2015, first ed.
Van Heteren, S., Fitzgerald, D.M., Barber, D.C., Kelley, J.T., Heteren, S. Van, Fitzgerald, D.M., Barber, D.C., Kelley, J.T., Belknap, D.F., van Heteren, S., Fitzgerald, D.M., Barber, D.C., Kelley, J.T., Belknap, D.F., 1996. Volumetric analysis of a New England barrier system using ground-penetrating-radar and coring techniques. J. Geol. 104, 471–483.
Van Heteren, S., Oost, A.P., van der Spek, A.J.F., Elias, E.P.L., 2006. Island-terminus evolution related to changing ebb-tidal-delta configuration: Texel, The Netherlands. Mar. Geol. 235, 19–33.
Valiente, N.G., Masselink, G., McCarroll, R.J., Scott, T., Conley, D., King, E., 2020. Nearshore sediment pathways and potential sediment budgets in embayed settings over a multi-annual timescale. Mar. Geol. 427, 106270.
Vieira da Silva, G., Toldo, E.E., Klein, A.H. da F., Short, A.D., Woodroffe, C.D., 2016. Headland sand bypassing - Quantification of net sediment transport in embayed beaches, Santa Catarina Island North Shore, Southern Brazil. Mar. Geol. 379, 13–27.
Vieira Da Silva, G.V., Muler, M., Prado, M.F.V., Short, A.D., Da Fontoura Klein, A.H., Toldo, E.E., 2016. Shoreline Change Analysis and Insight into the Sediment Transport Path along Santa Catarina Island North Shore, Brazil. J. Coast Res. 32, 863–874.
Vousdoukas, M.I., Ranasinghe, R., Mentaschi, L., Plomaritis, T.A., Athanasiou, P., Luijendijk, A., Feyen, L., 2020. Sandy coastlines under threat of erosion. Nat. Clim. Change 10, 260–263.
Wallace, D.J., Anderson, J.B., Fernández, R.A., 2010. Transgressive ravinement versus depth of closure: A geological perspective from the upper Texas coast. J. Coast Res. 26, 1057–1067.
Wallace, D.J., Anderson, J.B., 2013. Unprecedented erosion of the upper Texas coast: Response to accelerated sea-level rise and hurricane impacts. Bull. Geol. Soc. Am. 125, 728–740.
Walters, D., Moore, L.J., Duran Vinent, O., Fagherazzi, S., Mariotti, G., 2014. Interactions between barrier islands and backbarrier marshes affect island system response to sea level rise: Insights from a coupled model. J. Geophys. Res. Earth Surf. 119, 2013–2031.
Wikel, G.L., 2008. Variability in Geologic Framework and Shoreline Change: Assateague and Wallops Islands, Eastern Shore of Virginia. M.S. Thesis. Institute of Marine Science, Virginia.
Wilkinson, B.H., 1975. Matagorda Island, Texas: the evolution of a Gulf Coast barrier complex. Geol. Soc. Am. Bull. 86, 959–967.
Wright, E., Kruse, S., Forman, S.L., Harris, M.S., 2017. Millennial scale development of a southeastern United States spit. J. Coast Res. 34, 25.
Zăinescu, F.I., Tătui, F., Valchev, N.N., Vespremeanu-Stroe, A., 2017. Storm climate on the Danube delta coast: evidence of recent storminess change and links with large-scale teleconnection patterns. Nat. Hazards 87, 599–621.
Zăinescu, F.I., Vespremeanu-Stroe, A., Tătui, F., 2019. The formation and closure of the Big Breach of Sacalin spit associated with extreme shoreline retreat and shoreface erosion. Earth Surf. Process. Landforms 44, 2268–2284.
Zaremba, N., Mallinson, D.J., Leorri, E., Culver, S., Riggs, S., Mulligan, R., Horsman, E., Mitra, S., 2016. Controls on the stratigraphic framework and paleoenvironmental change within a Holocene estuarine system: Pamlico Sound, North Carolina, USA. Mar. Geol. 379, 109–123.